A novel mechanism of natural killer cell response to anti-CTLA-4 therapy identified by integrative analysis of mouse and human tumors

Emily F. Davis-Marcisak[1,2,6], Allison A. Fitzgerald[3,6], Michael D. Kessler[2], Ludmila Danilova[2], Elizabeth M. Jaffee[2], Neeha Zaidi[2], Louis M. Weiner[3], Elana J. Fertig[2,4,5,*]

Affiliations

1. McKusick-Nathans Institute of the Department of Genetic Medicine, Johns Hopkins School of Medicine, Baltimore, MD, USA

2. Department of Oncology, Sidney Kimmel Comprehensive Cancer Center, Johns Hopkins School of Medicine, Baltimore, MD, USA

3. Department of Oncology, Georgetown Lombardi Comprehensive Cancer Center, Georgetown University Medical Center, Washington, DC, USA

4. Department of Applied Mathematics and Statistics, Johns Hopkins University Whiting School of Engineering, Baltimore, MD, USA

5. Department of Biomedical Engineering, Johns Hopkins University School of Medicine, Baltimore, MD, USA

6. These authors contributed equally to this work

** Corresponding author*

Abstract

Immune checkpoint-inhibitory antibodies (ICIs) are well-established immunotherapies. Despite this, the impact of ICI therapy on non-T cell intratumoral immune cells is ill-defined, restraining the improvement of ICI efficacy. Preclinical murine models of human disease are infrequently validated in clinical trials, impairing the identification of novel biological factors impacting clinical ICI response. To address this barrier, we used our previously described computational approach that integrates high-throughput single-cell RNA sequencing datasets to identify known and novel cellular alterations induced by ICIs that are conserved in mice and humans. We found a signature of intratumoral natural killer (NK) cell activation that is enriched in anti-CTLA-4 treated mouse tumors and correlates with longer overall survival and is predictive of anti-CTLA-4 (ipilimumab) response in melanoma patients. We demonstrate that human NK cells express CTLA-4, which directly binds anti-CTLA-4. These data reveal a novel role for NK cells in anti-CTLA-4 treatment and present opportunities to enhance ICI efficacy. Importantly, we provide a new computational tool for onco-immunology that can identify and validate biological observations across species.

1 Introduction

Immune checkpoint receptors, such as cytotoxic T-lymphocyte-associated protein-4 (CTLA-4) and programmed cell death protein (PD-1), are inhibitory T cell receptors that attenuate T cell activity. Tumor cells escape immunosurveillance by expressing ligands that bind immune checkpoint receptors. Immune checkpoint-inhibitory antibodies (ICIs) represent a class of immunotherapies that have remarkable anti-tumor efficacy in several cancer types. Despite this, the clinical utility of ICIs is limited by the lack of response in most patients (intrinsic resistance), the emergence of resistance among those patients who initially respond (acquired resistance), and the inability to predict responders prior to treatment initiation. Combination strategies, such as the administration of both anti-CTLA-4 and anti-PD-1 antibodies, are being investigated to improve clinical efficacy (Dammeijer et al., 2017; Tang et al., 2018), but patient response rates remain limited (Larkin et al., 2015; Motzer et al., 2018; Overman et al., 2018). To date, approaches to understand the molecular mechanisms that drive the therapeutic efficacy of ICIs have largely focused on T cells. Accumulating evidence suggests that the development of anti-tumor immunity in response to ICI relies on other immune cell types within the tumor microenvironment - including natural killer (NK) cells. A better understanding of how these additional cellular populations contribute to ICI-mediated tumor regression is critical to identifying biomarkers of response and new therapeutic strategies to improve patient outcomes.

Despite being the first ICI to receive FDA approval (Hodi et al., 2010; Robert et al., 2011), the driving mechanism of action of anti-CTLA-4 antibodies (ipilimumab) is widely debated. Anti-CTLA-4 causes tumor regression by enhancing T cell effector activity by blocking CTLA-4 interactions with B7 ligands (Krummel and Allison, 1996; Sutmuller et al., 2001). However, recent studies in mice suggest that anti-CTLA-4 efficacy is dependent on the depletion of CTLA-4 expressing regulatory T cells (Du et al., 2018; Simpson et al., 2013). In these models, T cell depletion is mediated by the anti-CTLA-4 antibody Fc domain that interacts with Fc receptors expressed by many immune cell types, such as NK cells. This results in the lysis of CTLA-4 expressing regulatory T cells (Tregs) through antibody-dependent cellular cytotoxicity (ADCC) (Du et al., 2018; Simpson et al., 2013). However, the importance of ADCC is also subject to debate, as several publications have shown that depletion of Tregs is not a primary mechanism of action of anti-CTLA-4 therapy in both mice and humans (Ferrara et al., 2019; Kavanagh et al., 2008; Quezada et al., 2006; Schmidt et al., 2009). Additionally, while anti-CTLA-4 has been shown to bind most human Fc receptors, giving it the theoretical capacity to induce ADCC, a recent clinical study found that anti-CTLA-4 treatment does not deplete Tregs in several human cancer types (Sharma et al., 2019a). Therefore, a clear understanding of the mechanisms of action underlying anti-CTLA-4 and whether the same mechanisms are involved in mouse and human tumors remains elusive.

Preclinical mouse models are essential tools for identifying

potential therapies and elucidating biological mechanisms that underlie therapeutic success. Unfortunately, the majority of preclinical successes fail in clinical trials (Perel et al., 2007). The inability to translate findings from mouse models to human disease remains a critical challenge in cancer research. The emergence of single-cell RNA sequencing (scRNA-seq) technologies has made it possible to compare high-throughput mouse and human datasets to search for translatable features. Previous scRNA-seq studies have attempted to characterize conserved cell types or states in mouse and human cells by measuring marker genes whose expression correlates with cellular function (Brown et al., 2019; Crinier et al., 2018; Yu et al., 2019; Zilionis et al., 2019). Standard clustering methods that partition cells into discrete groupings according to their transcriptional profile is fundamental to this analysis. However, clustering methods typically capture predominant signals in a dataset, thereby limiting the ability to unravel gene expression programs that dictate cell type identity (i.e., NK versus Treg) from cell state (i.e., activated versus resting) (Kotliar et al., 2019). In addition, when datasets are obtained from different studies (i.e., human versus mouse), they often contain batch effects that need to be corrected prior to meta-analyses. These challenges are especially relevant to the complex molecular alterations present across heterogeneous populations of cells within the tumor immune microenvironment during ICI response (Kiselev et al., 2019).

To address these shortcomings and improve translational advances, we previously developed a computational framework that utilizes two complementary machine learning methods to translate relationships across independent datasets from different species. This approach first uses matrix factorization to identify transcriptional signatures within a reference scRNAseq dataset. In contrast to clustering methods, the transcriptional signatures from factorization methods can simultaneously distinguish cell type identities and state transitions. Transfer learning is then used to integrate the transcriptional signatures learned from the original dataset into a new dataset to assess if the molecular and cellular processes are conserved. In the context of development, we have shown that this approach is able to identify cell types and biological processes shared between the developing retina in mice and humans (Stein-O'Brien et al., 2019). Here, we extend this approach to identify transcriptional alterations in intratumoral immune cells induced by ICI treatment that are conserved in mice and humans. We found distinct gene expression signatures and cellular transitions associated with different ICIs that led to tumor progression or rejection. We focus our analysis on a signature of NK cells that predicted the therapeutic success or failure of anti-CTLA-4 and use molecular techniques to validate computational findings and novel mechanisms.

2 Results

CoGAPS identifies known molecular alterations in response to immunotherapy from scRNA-seq data

In scRNA-seq, each cell's transcriptional profile is reflective of cell type and cell state. Clustering methods reduce all cells in a cluster to a single shared transcriptional profile, which can mask these biological differences. In contrast, matrix factorization methods allow cells to associate with multiple gene expression signatures and accurately identifies signatures for both cell type identity and cellular activity (i.e., immune activation) from scRNA-seq data (Kotliar et al., 2019; Puram et al., 2017; Stein-O'Brien et al., 2019). When combined with the machine learning concept transfer learning, these signatures can be used to apply a priori knowledge gained from one dataset to another distinct but related dataset. We previously developed such an approach that combines our matrix factorization method, CoGAPS, with our transfer learning technique, projectR (Stein-O'Brien et al., 2019). In the current study, we sought to establish whether transcriptional signatures from mouse tumor models treated with ICIs were translatable to human tumors treated with ICIs. Briefly, we first applied CoGAPS to identify patterns of therapy-induced alterations from a scRNA-seq dataset of a mouse tumor model. In this context, the patterns identified by CoGAPS are reflective of transcriptional signatures. We then used projectR to project the mouse patterns into multiple human datasets (Fig. 1A). Importantly, patterns shared between datasets are preserved in this analysis, while patterns associated with technical artifacts or batch effects drop out. Patterns that exhibit robust replication across datasets represent conserved tumor biology in murine and human tumor settings.

To determine the molecular changes induced by ICIs in a preclinical mouse model, we first applied CoGAPS to a publicly available scRNA-seq dataset of 15,000 immune cells isolated from mouse sarcomas (Gubin et al., 2018). These tumors were treated with control monoclonal antibodies, anti-PD-1, anti-CTLA-4, or combination anti-PD-1 and anti-CTLA-4 antibodies (Fig. 1B). A critical challenge in matrix factorization algorithms such as CoGAPS is the selection of an appropriate dimensionality, or number of patterns, to resolve biological features from the data (Stein-O'Brien et al., 2018). Therefore, we ran this algorithm across multiple-dimensionalities. Consistent with previous studies, we found that different biological processes were captured at different dimensionalities (Way et al., 2019). Although unsupervised, when detecting 3 patterns this analysis revealed a hierarchy of immune cell type specification that distinguishes myeloid from lymphoid lineages (Supplemental Fig. 1). When we increased the number of patterns analyzed in this data to 21, we retained this lineage distinction and also captured additional patterns associated with distinct immune cell types (Fig. 1C).

To confirm the biological significance of our CoGAPS identified patterns, we assessed the transcriptional signatures identified in ICI treated mouse sarcomas for known cellular alterations relevant to immunotherapy. For example, pattern 13 was enriched in macrophages/monocytes from progressing tumors treated with control monoclonal antibody (Fig. 1D and E) while pattern 12 was prevalent in macrophages/monocytes from tu-

mors treated with anti-PD-1 (Fig. 1F and G). To identify specific attributes captured in each pattern, we performed gene set analysis using the gene weights for each pattern as input. We used the hallmark gene sets from the Molecular Signatures Database (MSigB) (Liberzon et al., 2015) and the PanCancer Immune Profiling gene panel from Nanostring Technologies to assess enrichment of gene sets controlling well-defined biological processes. Gene set statistics for all patterns are provided in supplemental Table 1. Macrophages are commonly divided into two subsets, pro-inflammatory M1 and anti-inflammatory M2, which are generally considered to be anti-tumor and pro-tumor, respectively (Lu et al., 2019). As expected, pattern 13 in control-treated cells was enriched for M2 macrophage polarization, which promotes tumor growth and metastasis ($p < 1 \times 10^{-2}$, Supplemental Table 1). In contrast, pattern 12 in anti-PD-1 treated cells was enriched for M1 macrophage polarization and interferon responses ($p < 1 \times 10^{-2}$, Supplemental Table 1). This finding agrees with a recent study, which showed that anti-PD-1 treatment leads to a functional transition within the macrophage compartment towards an immunostimulatory M1 phenotype (Xiong et al., 2019).

CoGAPS analysis identifies a subset of activated NK cells in mouse tumors treated with anti-CTLA-4

In addition to the known molecular and cellular pathways that CoGAPS identified in immune cells from ICI treated mouse tumors, we identified an unanticipated transcriptional signature that was specific to NK cells (Fig. 2A and B). This signature was captured by pattern 7, and the presence of high levels in only a subset of NK cells suggested that it was related to cell state rather than cell type. While tumors from each treatment group contained NK cells with elevated levels of pattern 7, there was a significant enrichment in NK cells from tumors that were treated with anti-CTLA-4 (Fig. 2C). We next used the CoGAPS PatternMarker statistic (Stein-O'Brien et al., 2017) to identify genes strongly associated with each pattern. PatternMarker analysis identified 3,195 genes associated with pattern 7. Gene set enrichment analysis of these genes revealed an upregulation of interferon-gamma and IL2-STAT5 gene sets, which are key pathways that govern cytotoxicity and maturation in NK cells (Supplemental Table 1, $p < 1 \times 10^{-2}$) (Gotthardt and Sexl, 2016).

To further explore whether pattern 7 was identifying cells undergoing functional state changes in response to ICI, we performed pseudotime analysis on intratumoral NK cells treated with anti-CTLA-4 (Trapnell et al., 2014). This analysis enables a quantitative estimation of cellular progression through dynamic biological processes. The pseudotemporal ordering showed a sequential progression in cellular trajectory during anti-CTLA-4 treatment (Figure 2D). This pseudotemporal trajectory was highly correlated with the pattern 7 weight identified in each cell (0.71 spearman correlation). Notably, the trajectory revealed a single transition state as a result of anti-CTLA-4 treatment, with individual cells having transcriptional profiles that reflect various points along the trajectory. Differential expression analysis across pseudotime identified 1,968 genes with significant changes (q value < 0.01) in gene expression during exposure to anti-CTLA-4 (Supplemental Table 2). We then looked for differentially expressed genes over pseudotime that were strongly associated with pattern 7 as determined by patternMarker analysis (Fig. 2E). The 148 differentially expressed genes included markers of NK cell activation, such as perforin, granzymes, and Ly6a (Lanier, 2000), which significantly increased in expression during the pseudotime trajectory as a result of anti-CTLA-4 treatment (Fig. 2F). These data support recent findings that NK cells within mouse tumors can be functionally modulated by ICI treatment (Hsu et al., 2018; Sanseviero et al., 2019).

Preclinical NK cell activation signature is associated with overall survival in metastatic melanoma patients

To evaluate the clinical relevance of pattern 7, the NK cell activation signature, we used patient samples from The Cancer Genome Atlas (TCGA) to test for an association between pattern 7 and overall survival. We first used our transfer learning method projectR (Sharma et al., 2019b) to project our 21 transcriptional patterns associated with ICI treatment into RNAseq data from 9,553 TCGA tumors representing 32 cancer types (Cancer Genome Atlas Research Network et al., 2013). We next fit a multiple linear regression model to estimate the association between the projected weight of each transcriptional pattern and overall cancer survival. When including cancer type as a covariate in the model given its significant effect on survival, we identified pattern 7 to be the transcriptional pattern most significantly associated with overall survival (Fig. 3A, $p < 6 \times 10^{-5}$). We also found that pattern 15 was significantly associated with overall survival (Fig. 3A, $p < 5.9 \times 10^{-4}$), which was highest in a subset of mouse NK cells and proliferating lymphocytes similar to pattern 7 (Supplemental Fig. 2A, Fig. 2B). When including age as a covariate in our linear model, given its influence on overall survival, pattern 7 remains the most significantly associated with overall survival (Supplemental Fig. 2B, $p < 1.6 \times 10^{-4}$). Interestingly, when testing the relationship between the transcriptional patterns and age at diagnosis, pattern 7 was the only pattern showing a significant negative association (Supplemental Fig. 2C, $p < 6.7 \times 10^{-3}$). Several studies have reported age-related alterations in NK cell function, including a decreased ability to proliferate and kill target cells in older individuals (Hazeldine and Lord 2013; Gounder et al. 2018). The signature of NK cell activation appears to similarly decrease as individuals age, which may have implications for cancer incidence in elderly individuals.

These findings indicate that the role of NK cells in tumor immunity needs to be reconsidered in a broader context. When fitting separate regression models per cancer type, we found that melanoma (SKCM) had the strongest and most significant association between pattern 7 and overall survival (Fig. 3B, Supplemental Fig. 2D, $p < 5 \times 10^{-3}$). Notably, this association was driven entirely by the melanoma metastases samples (Supplemental Fig. 2E, F), which is consistent with the role of NK cells controlling cancer progression and metastasis (López-

Soto et al., 2017). Pattern 7 was also able to stratify metastatic melanoma patients within the context of a survival analysis when comparing patients with the highest pattern 7 weights (top 5%) to other patients (Fig. 3C). Prostate cancer (PRAD) and breast cancer (BRCA) also had modestly significant positive associations between pattern 7 and overall survival ($p < 0.05$). Importantly, these results demonstrate that transcriptional patterns of ICI response are translatable across species from preclinical to clinical data and agree with previous studies that indicate NK cell activation is important to overall survival in metastatic melanoma (Cursons et al., 2019).

CTLA-4 expression is positively correlated with the infiltration of active NK cells in immunogenic human tumors

Given that pattern 7 was associated with a subset of NK cells from mice treated with anti-CTLA-4, we hypothesized that there may be a correlation between CTLA-4 expression and intratumoral NK cell content. To explore this hypothesis, we used CIBERSORT to infer immune cell proportion across 6 immunogenic solid tumor types from TCGA, skin cutaneous melanoma (SKCM), kidney renal clear cell carcinoma (KIRC), cervical kidney renal papillary cell carcinoma (KIRP), squamous cell carcinoma of the lung (LUSC), lung adenocarcinoma (LUAD), and bladder carcinoma (BLCA). When running CIBERSORT, we used the LM22 signature matrix designed by Newman et al (Newman et al., 2015) to estimate the relative fraction of 22 immune cell types within input mixture samples, which include an estimation of resting and activated NK cell proportions (Fig. 3D). Correlation analysis between CTLA-4 expression and CIBERSORT cell type estimation revealed that the direction of correlation in NK cells was dependent upon the activation state (Fig. 3E, Supplemental table 3). Across several tumor types, activated NK cells were positively correlated with CTLA-4 expression while resting NK cells were negatively correlated. CTLA-4 expression was negatively correlated with estimated proportions of resting NK cells in SKCM ($p < 1 \times 10^{-4}$), BLCA ($p < 1 \times 10^{-3}$), LUSC ($p < 1 \times 10^{-2}$), KIRP ($p < 1 \times 10^{-2}$), and KIRC ($p < 1 \times 10^{-9}$). On the other hand, activated NK cells were positively correlated with CTLA-4 expression in SKCM ($p < 1 \times 10^{-6}$), BLCA ($p < 1 \times 10^{-2}$), LUSC ($p < 0.05$), KIRP ($p < 0.05$), and KIRC ($p < 1 \times 10^{-2}$). In agreement with the current understanding of CTLA-4 biology, CTLA-4 expression was also positively correlated with the estimated proportions of Tregs in each tumor type (Supplemental Table 3).

Preclinical NK cell activation signature is associated with ipilimumab response in metastatic melanoma patients

Given that anti-CTLA-4 appears to promote NK cell activation, we next investigated the relevance of the NK cell activation signature, pattern 7, to immunotherapy responses in metastatic melanoma patients. Using the same approach we used to project patterns into TCGA tumors, we queried the mouse patterns in two independent scRNA-seq datasets of metastatic melanoma patients treated with ICIs (de Andrade et al., 2019; Sade-Feldman et al., 2018). First, we analyzed a scRNA-seq dataset of 16,000 immune cells isolated from melanoma metastases. Patients in this study were treated with anti-PD-1, anti-CTLA-4, or combination anti-PD-1 and anti-CTLA-4 antibodies, and the biopsies were taken either prior to or during treatment (Sade-Feldman et al., 2018). We projected this scRNAseq data into the 21 CoGAPS patterns derived from the mouse sarcoma intratumoral immune cell data. Using the projected pattern weights and treatment outcomes, we evaluated the ability of each pattern to distinguish signatures associated with therapeutic response in the human dataset. We found that in pre-treatment biopsies, pattern 7 was significantly higher in tumors responsive to anti-CTLA-4 compared to non-responsive tumors ($p < 1 \times 10^{-15}$, Supplemental Fig. 3A). This is particularly notable given that pattern 7 was strongly associated with NK cells treated with anti-CTLA-4 in the mouse data. To further examine this relationship, we tested for enrichment of pattern 7 in NK cell populations from this human dataset. While NK cells were not annotated in the study that produced this data (Sade-Feldman et al. 2018), we observed that cells expressing key NK marker genes were intermixed with T cells in the lymphocyte cluster (Supplemental Fig. 3B). This is consistent with previous scRNA-seq studies that have identified subpopulations of T cells that express transcripts linked to the cytotoxic function of NK cells, such as NKT cells (Patil et al., 2018; Smith et al., 2020). Thus, to eliminate T cells, we performed a gene expression gating strategy that required expression of several transcripts related to NK cell function (NCR1, NKG7, and FCGR3A) and a lack of the T cell transcripts (CD4, CD3D, and CD3G). Gating for NK cells confirmed that pattern 7 was enriched in intratumoral NK cells isolated from anti-CTLA-4 responsive tumors (Fig. 4A, $p < 1 \times 10^{-8}$). Importantly, these cells were obtained from tumor biopsies prior to the administration of anti-CTLA-4, which suggests that cytotoxic NK cell infiltration is a predictive biomarker of therapeutic response. In patients treated with anti-PD-1, there was no significant difference in pattern 7 weights between responders and non-responders regardless of whether biopsies were taken before (Fig. 4A, $p > 0.05$) or during (Fig. 4B, $p > 0.05$) treatment. In contrast, pattern 7 was significantly enriched in tumors responsive to combination anti-CTLA-4 and anti-PD-1 taken before (Fig. 4A, $p < 0.05$) and during (Fig. 4B, $p < 0.01$) treatment. Using receiver operating characteristic curve (ROC) analysis, we found that pattern 7 weight had a moderate ability to classify anti-CTLA-4 response (Fig. 4C), suggesting that the NK activation signature has the potential utility to predict responsiveness to anti-CTLA-4 from pre-treatment tumor biopsies. While this dataset lacked data from biopsies taken during anti-CTLA-4 treatment, these findings indicate that the presence of active NK cells within tumors is important to the clinical usage and success of anti-CTLA-4 therapies.

Although ICI therapy can lead to durable responses in patients with metastatic melanoma, intrinsic and acquired resistance remain major causes of mortality (Jenkins et al., 2018). To determine the relationship between pattern 7 and mechanisms of therapeutic resistance, we next projected the transcriptional

patterns into a dataset of NK cells isolated from melanoma metastases and matching blood samples of patients that had progressed after immunotherapy (de Andrade et al., 2019). This dataset included two patients that had an initial response to ICI (acquired resistance), two patients that failed to respond to ICI (intrinsic resistance), and one patient that was not given ICI (untreated). We found high pattern 7 weights in a subset of intratumoral NK cells from the two patients who had an initial response to ICI (Fig. 4D). Consistent with our results which indicate that pattern 7 is enriched in NK cells from anti-CTLA-4 responsive tumors, we found that the highest projected pattern 7 weights were in NK cells from the patient responsive to anti-CTLA-4 (ipilimumab). Elevated pattern 7 weights were also found in the patient responsive to combination treatment with anti-PD-1 and oncolytic virus (pembrolizumab + TVEC). Notably, this observation was specific to intratumoral NK cells, as cells with elevated pattern 7 weight were absent in NK cells isolated from matched peripheral blood samples (Fig. 4E). This result indicates that anti-CTLA-4 treatment leads to NK cell activation specifically within the tumor microenvironment, consistent with observations in mice (Sanseviero et al., 2019).

CTLA-4 is expressed by both human NK cell lines and healthy human donor-derived NK cells.

In mice, NK cells express CTLA-4 when activated with IL-2 (Stojanovic et al., 2014). We hypothesized CTLA-4 is similarly expressed by human NK cells and that anti-CTLA-4 could activate NK cells by blocking CTLA-4. To investigate this possibility, we first assessed the expression of CTLA-4 transcripts in NK cells from scRNA-seq data. Indeed, some intratumoral NK cells in mice and humans express CTLA-4 as well as high levels of cytotoxic genes (GZMB and NKG7) (Fig. 5A). This indicates that NK cells, particularly those with an activated phenotype, express CTLA-4. It has been previously demonstrated that NK cells can express other immune checkpoints, such as PD-1 (Concha-Benavente et al., 2018; Hsu et al., 2018). Consistent with this, we found a few cytotoxic NK cells that similarly express PD-1 (Supplemental Fig. 4). Importantly, if the expression of CTLA-4 and PD-1 is low to moderate in NK cells, these genes could suffer from poor capture efficiency and dropout during scRNA-seq (Chen et al., 2019). These technical limitations could result in the observed detection in only a handful of NK cells.

To confirm that human NK cells express CTLA-4, we directly tested four human NK cell lines (NK-92, NKL, YT, and KHYG-1) for CTLA-4 expression at the RNA and protein level. While all four cell lines appeared negative for CTLA-4 by flow cytometry (Fig. 5B), all NK cell lines revealed robust CTLA-4 expression determined by western blot and qRT-PCR (Fig. 5C and D). Previous studies have characterized two distinct isoforms of CTLA-4, a transmembrane dimerized full-length CTLA-4 isoform that weighs approximately 48-50 kDa, and a soluble CTLA-4 monomeric isoform that weighs approximately 28-30 kDa (Darlington et al., 2005; Esposito et al., 2014). We observed both the dimerized and monomeric isoforms by western blot (Fig. 5D). Since CTLA-4 is known to be expressed on several tumor-derived human cell lines (Contardi et al., 2005; Pistillo et al., 2003) we wanted to exclude the possibility that this observation was specific to malignant NK cells so we assessed CTLA-4 expression in unstimulated ex vivo CD56+ NK cells isolated from healthy human donor PBMCs. Western blot and rt-qPCR confirmed that NK cells from each donor constitutively expressed CTLA-4 (Figure 5E and F). The robust expression of CTLA-4 by human NK cells supports our hypothesis that the activation phenotype observed in mouse and human scRNA-seq data is the result of anti-CTLA-4 modulating NK cell activity by directly binding to CTLA-4 on the NK cell surface.

Ipilimumab binds to CTLA-4 expressed on the NK cell surface independent of CD16.

We next wanted to determine if ipilimumab specifically was capable of binding to CTLA-4 expressed on the NK cell surface. Human NK cells also express the cell surface Fc receptor CD16 (FcRIIIA), which is capable of binding to the Fc domain of IgG1 and IgG3 antibodies (Simmons and Seed, 1988). When CD16-expressing NK cells recognize an Fc domain they become active, release cytokines, degranulate, and lyse the target cell. To demonstrate that ipilimumab, an IgG1 antibody, could recognize CTLA-4 on NK cells we used the human NK cell line NK-92, which lacks CD16 expression (Fig. 6A) to exclude the possibility of Fc receptor binding by ipilimumab. Immunofluorescence imaging demonstrated that fluorescently labeled anti-CTLA-4, but not the IgG control, was capable of binding to NK-92 through recognition of CTLA-4 on the surface (Fig. 6B). The specificity of the stain was confirmed using the CTLA-4 null line PANC-1 (Supplemental Fig. 4). To the best of our knowledge, this is the first demonstration that anti-CTLA-4 can directly interact with human NK cells via a CD16-independent mechanism. This suggests the NK cell activation signature observed in anti-CTLA-4 responsive tumors could be mediated by anti-CTLA-4 antibody binding to CTLA-4 expressing NK cells.

NK cells coexpress CD28 and CTLA-4

After identifying that anti-CTLA-4 binds to human NK cells independent of CD16, we hypothesized that anti-CTLA-4 induces NK cell activation in a manner similar to CD4+ T cells activation. In CD4+ T cells, CTLA-4 is co-expressed with CD28 and CTLA-4 competes with CD28 for the ligands B7.1 (CD80) and B7.2 (CD86). To test if this working hypothesis could be applied to NK cell biology, we first investigated CD28 surface expression in multiple human NK cell lines by flow cytometry. Of the four cell lines tested, two cell lines (NK-92 and YT) expressed CD28 on the surface and two cell lines (NKL and KHYG-1) did not have detectable levels of CD28 on the surface (Fig. 7A). In addition to flow cytometry, we used qRT-PCR to investigate mRNA expression levels in human NK cell lines. By qRT-PCR, three of the four NK cell lines (NK-92, YT, and KHYG-1) had detectable levels of CD28 mRNA (Fig. 7B). We also saw that CD56+ NK cells isolated from healthy human donor PBMCs also expressed CD28 by qRT-PCR (Fig. 7C). This finding confirms previous reports that human NK cells express CD28 (Galea-Lauri et al.,

1999).

Activated T cells co-express CD28 and CTLA-4 (Chambers et al., 2001). To determine if NK cells also co-express CD28 and CTLA-4, we performed a correlation analysis between the expression of CD28 and CTLA-4 in the scRNA-seq data of human NK cells isolated from melanoma metastasis (de Andrade et al., 2019). Indeed, we found a positive correlation ($R^2 = 0.33$, $p = 0$) between CD28 and CTLA-4 transcripts in tumor-infiltrating NK cells from scRNA-seq data (Fig. 7D). As previously described, NK cells that express CTLA-4 were restricted to a population of cells with an active, cytotoxic phenotype (Fig. 5A). Thus, active intratumoral NK cells appear to co-express CTLA-4 and CD28 at the RNA level, supporting a parallel role for these receptors in T cells and NK cells.

Previous studies have demonstrated that human NK cells are capable of binding to B7 expressing target cells in vitro in a manner that is dependent on CD28-B7 interactions (Luque et al., 2000; Martín-Fontecha et al., 1999; Wilson et al., 1999). However, the extent to which malignant cells express B7 remains unclear. To assess the relevance of B7 expression in human cancers, we used RNA-seq data to compared B7.2 (CD86) expression in tumor versus paired normal tissue (TCGA) and found that 14 solid tumors, including melanoma, had significantly higher B7 expression in tumors compared to normal tissue (Fig. 7E). To rule out the possibility that the increased tumor B7 expression was attributed to immune infiltrate present in the bulk TCGA samples, we assessed B7 expression in RNA-seq data from malignant cell lines and found B7 expression in multiple cancer cell line types (Supplementary Figure 5). Of note, melanoma cell lines had the highest B7 expression of all solid malignancy lines. These findings are supported by previous reports of B7.1 and B7.2 expression in several mouse tumor cell lines (melanoma and colorectal carcinomas) (Tirapu et al., 2006) and human tumor cell lines (gastric, esophageal and colorectal carcinomas) (Li et al., 1996) human colon preneoplastic epithelial cells (Marchiori et al., 2019).

CD4+ T cells are inactivated upon CTLA-4 recognition of B7. Since we demonstrated NK cells express CTLA-4 and tumor cells express B7, we hypothesized that NK cell activation would be inhibited by high B7 expression in tumors. To test this hypothesis, we assessed the correlation between our CoGAPS-identified immune cell patterns, including pattern 7, which is indicative of activated NK cells, and B7 expression in TCGA data. We found a negative correlation between pattern 7 and B7 expression, which demonstrates that higher B7 expression is associated with lower NK cell activation (Fig. 7F). Taken together, our data support a model whereby anti-CTLA-4 antibodies block CTLA-4-B7 interactions resulting in enhanced NK cell activation (Fig. 7G).

3 Discussion

Here, we integrate state-of-the-art machine learning algorithms and molecular biology approaches to identify a novel association between NK cells and immunotherapy outcomes. The ability of our matrix factorization algorithm, CoGAPS, to identify continuous cell states enabled the discovery of an association between NK cell activation and anti-CTLA-4 response in mouse sarcomas. While Gubin et al. was previously unable to detect this relationship using clustering methods, the authors were able to identify marked upregulation of NK cell granzyme expression specific to anti-CTLA-4 treatment after analyzing paired mass cytometry (Gubin et al., 2018). Our results demonstrate that the presence of NK cell activation in response to anti-CTLA-4 was detectable from the scRNA-seq data alone, as CoGAPS was able to identify this response directly, without the need for clustering and differential expression analyses. This highlights the advantages of CoGAPS over standard analysis pipelines and its potential to generate previously unidentified discoveries from publicly available scRNA-seq data. Using our transfer learning approach, projectR, we were able to project patterns across species into clinical data from melanoma patients to reveal cancer immunotherapy mechanisms conserved between different species, tumor types, and which correlate with overall survival and ICI responsiveness. Despite known differences in mice and human NK cell surface receptors (Murphy et al. 2012), our approach was able to identify a conserved signature of NK cell effector function relevant to clinical outcomes by analyzing homologous genes. This supports the continued observation that key biological roles of NK cells are shared between species (Murphy et al. 2012). Of note, this study provides the first evidence that transfer learning can go beyond the identification of conserved developmental processes (Stein-O'Brien et al., 2019) to elucidate complex onco-immunological biology.

A number of immune checkpoints are expressed by both T cells and NK cells. For example, recent studies have found that NK cells within several human and mouse tumor types express PD-1, and that ligands for these checkpoint receptors negatively regulate NK cell activity (Kim and Kim, 2018; Mariotti et al., 2019). Consistent with this, blocking PD-1 receptors with anti-PD-1 therapy enhances NK cell-mediated anti-tumor responses (Hsu et al., 2018), and NK cell infiltration correlates with clinical responsiveness to anti-PD-1 therapy (Barry et al., 2018). Despite growing evidence for the role of checkpoint receptors in NK mediated anti-tumor responses, the expression of CTLA-4 by NK cells has been disputed in the literature. While mouse NK cells inducibly express CTLA-4 in response to IL-2 (Stojanovic et al., 2014), a recent study was unable to detect CTLA-4 on the surface of intratumoral murine NK cells (Sanseviero et al., 2019). An earlier study in humans also demonstrated an absence of surface CTLA-4 expression in NK cells from healthy human donors (Lang et al., 1998). Contrary to these earlier reports, our results demonstrate CTLA-4 is constitutively expressed by circulating healthy donor NK cells and can also be expressed by intratumoral NK cells. One possible explanation for why previous studies failed to identify the expression of CTLA-4 by human NK cells is the reliance on flow cytometry in these studies. Flow cytometry can be limited by challenges related to the generation of antibodies and further complicated

by the rapid surface expression dynamics of CTLA-4 (Valk et al., 2008). In support of this explanation, we too fail to detect intracellular or surface CTLA-4 expression when using flow cytometry (Fig. 5B), even though we are able to unequivocally demonstrate CTLA-4 expression at the RNA and protein level by qRT-PCR and western blot in ex vivo unstimulated healthy donor NK cells (Fig. 5E and F), as well as surface expression using immunofluorescence (Fig. 6B).

Regardless of the reported lack of expression, several reports highlight an interesting relationship between NK cells and anti-CTLA-4 response in humans. In melanoma patients treated with anti-CTLA-4, a higher percentage of circulating mature NK cells is correlated with improved overall survival, and NK cells isolated from responsive patients have increased cytolytic activity compared to NK cells isolated from non-responders (Tallerico et al., 2017). A very recent study also showed that an anti-CTLA-4-EGFR immunoconjugate enhances the in vitro lysis of breast cancer cells by NK cells (Passariello et al., 2020). In B16 melanoma models, NK cells and CD8+ T cells synergistically clear tumors in response to anti-CTLA-4 and IL-2 treatment (Kohlhapp et al., 2015). Furthermore, anti-CTLA-4 has been shown to increase transcriptional markers of NK cell cytotoxic activity in CT26 colon carcinoma tumors (Sanseviero et al., 2019). In aggregate, those studies did not provide mechanistic bases for the identified associations.

In contrast, the work reported here provides a mechanistic basis for the relationship between NK cells and the anti-CTLA-4 response in humans. Specifically, we provide a rationale for the activation of NK cells by anti-CTLA-4 molecules by demonstrating that NK cells constitutively express CTLA-4 on their cell surfaces and bind anti-CTLA-4. Consistent with previous studies (Azuma et al., 1992; Galea-Lauri et al., 1999), we show that human NK cells express CD28, a co-stimulatory receptor that competes with CTLA-4 for the binding of B7 ligands. The expression of B7 on tumor cells also enhances NK recognition and lysis of tumors through CD28-B7 interactions (Azuma et al., 1992; Chambers et al., 1996; Galea-Lauri et al., 1999; Luque et al., 2000; Martín-Fontecha et al., 1999; Terrazzano et al., 2002; Wilson et al., 1999). In intratumoral NK cells, CTLA-4 expression is correlated with the expression of genes associated with NK cell activation and proliferation as well as CD28. Suggesting that CTLA-4 functions in NK cells and effector T cells in a similar manner (Rowshanravan et al., 2018). This model is further supported by the observation that the NK cell activation signature, pattern 7, is present in anti-CTLA-4 responsive tumors prior to anti-CTLA-4 treatment. This suggests that NK cells must already be activated within the tumors and express CTLA-4 to get improved tumor clearance by the addition of anti-CTLA-4. Based on these observations, we infer that CTLA-4 may act as an immune checkpoint in NK cells and that anti-CTLA-4 enables sustained NK cell activation.

Beyond this novel mechanism of action, these findings have significant implications for the role of NK cells in anti-CTLA-4 clinical outcomes. In metastatic melanoma patients, we found that NK cell activation status prior to treatment correlates with clinical anti-CTLA-4 response. This indicates that NK cell transcriptional state has the potential to be used as a predictive biomarker. The elevated pattern 7 signature was observed in tumors responsive to anti-CTLA-4 alone or in combination with anti-PD-1, suggesting that this signature of NK cell activation is a specific response to therapies that include anti-CTLA-4. Importantly, given that pattern 7 did not associate with response to anti-PD-1 alone, this signature is unlikely to be due to NK cell activation mediated by Fc receptors binding to the Fc region of antibodies. In the context of therapeutic resistance, we detect NK cells with high expression of the activation signature in patients that developed acquired, but not primary, resistance to immunotherapy. This demonstrates that this signature is able to identify patients that had an initial response to therapy. Consistent with this signature being related to NK cell-mediated anti-CTLA-4 response, we observed the highest levels of this signature in intratumoral NK cells isolated from a patient initially responsive to anti-CTLA-4 but was absent in patients that were unresponsive to anti-PD-1 alone or in combination with anti-CTLA-4. Interestingly, this signature was also elevated in a patient initially responsive to combination anti-PD-1 and oncolytic virus. This could be due to the fact that infection of tumors with oncolytic viruses can result in NK cell activation that may stimulate NK-mediated anti-tumor immunity (Alvarez-Breckenridge et al., 2012). Furthermore, since this observation was specific to intratumoral NK cells and not circulating NK cells, approaches to transcriptionally profile patients using peripheral blood may be limited in identifying signatures relevant to clinical outcomes. It will be important for future studies to determine the specific function(s) of CTLA-4 in NK cell biology and the contribution of NK cell activation to immunotherapy response and resistance.

In summary, this work provides first mechanistic evidence that anti-CTLA-4 binds directly to human NK cells via recognition of CTLA-4 on the NK cell surface. We found that anti-CTLA-4 elicits a cytotoxic NK cell response conserved between mice and humans and is associated with clinical outcomes in metastatic melanoma. These findings suggest that NK cells play a significant role in patient response to anti-CTLA-4 therapy, and that this response is dependent on the pretreatment transcriptional state of the NK cells within the tumor microenvironment. We propose that, along with T cells, NK cells also participate in the clinical benefit of anti-CTLA-4 therapy. These observations suggest that therapies aimed at enhancing and recruiting NK cells within tumors may prove to have orthogonal benefits when combined with anti-CTLA-4 by helping to support T cell infiltration (Shimasaki et al., 2020) and/or by eliminating tumor subclones with antigen presentation defects (Nicolai 2020). This could be especially beneficial for patients whose tumor cells have been selected for loss of MHC expression by previous ICI treatment (Rodig et al., 2018; Sade-Feldman et al., 2017; Zaretsky et al., 2016). Importantly, this work demonstrates the utility of hybrid approaches combining computational

and molecular biology to advance our understanding of cancer immunotherapy and provides a template for future studies to investigate conserved therapeutic response mechanisms in mice and humans for other drugs and diseases.

4 Methods

Data collection

In this study, we used three public scRNA-seq datasets generated by different groups using droplet-based profiling technologies. Read counts for each scRNA-seq dataset were obtained from NCBI's Gene Expression Omnibus.

For CoGAPS analysis on preclinical immunotherapy samples, we used a scRNA-seq dataset containing 15,000 flow-sorted CD45+ intratumoral cells from mouse sarcomas that were collected during treatment with either control monoclonal antibody, anti-CTLA-4, anti-PD-1, or combination anti-CTLA-4 and anti-PD-1 (Gubin et al., 2018). This data was acquired with the 10x Genomics Chromium platform, using v1 chemistry. The accession number for this dataset is GSE119352.

For transfer learning, we used two human scRNA-seq datasets of intratumoral immune cells from metastatic melanoma patients. To first test the relationship between our preclinical CoGAPS patterns and clinical outcome, we used a scRNA-seq dataset containing 16,000 flow-sorted CD45+ intratumoral cells obtained from 48 human melanoma tumor biopsies from 32 patients at baseline or after treatment with either anti-CTLA-4, anti-PD-1, or combination anti-CTLA-4 and anti-PD-1 (Sade-Feldman et al., 2018). This data was acquired with Smart-seq2. The accession number for this dataset is GSE120575.

Next, to confirm the observed relationship between our preclinical NK activation signature and response to anti-CTLA-4, we used a scRNA-seq dataset containing 40,000 flow-sorted NK cells from matched blood and tumor samples obtained from 5 patients with melanoma metastases (de Andrade et al., 2019). Two patients had an initial response to treatment with anti-CTLA-4 or anti-PD-1 with oncolytic virus. Two patients failed to respond to combination anti-CTLA-4 and anti-PD-1 or anti-PD-1. One patient was not treated with immunotherapy. This data was acquired with the 10x Genomics Chromium platform, using v2 chemistry. The accession number for this dataset is GSE139249.

In addition, bulk RNA-seq was downloaded from The Cancer Genome Atlas (Cancer Genome Atlas Research Network et al., 2013). In this case, level 3 RSEM normalized across 33 tumor types were accessed from the Broad Institute TCGA GDAC Firehose (http://gdac.broadinstitute.org/runs/stddata__2016_01_28/data/) and log2-transformed. CIBERSORT scores for this data were obtained from Thorsson et al. (Thorsson et al., 2018).

These datasets were used for pattern discovery and transfer learning as described below.

Dimensionality reduction and cell type identification

Cell type inference analyses were performed for the Gubin et al. dataset with the standard Monocle3 workflow using package version 0.2.0. Dimensionality reduction and visualization for scRNA-seq data were performed using Uniform Manifold Approximation and Projection (UMAP) (McInnes et al., 2018). Briefly, the first 15 principal components were used as input into the reduce_dimension function. Canonical cell type marker genes as described in Gubin et al. were used to annotate cells (Gubin et al., 2018).

Mouse pattern discovery and gene set analysis using CoGAPS

CoGAPS analysis was performed using the R/Bioconductor package CoGAPS version 3.5.8 to analyze the mouse sarcoma dataset from Gubin et al. (Gubin et al., 2018). Genes with a standard deviation of zero were removed prior to analysis. The log2 transformed count matrix of remaining genes across all samples was used as input to the CoGAPS function. Default parameters were used, except nIterations = 50,000, sparseOptimization = True, nSets = 12. The input parameters for nPatterns was determined empirically, by testing over a range of dimensions. When the nPatterns input was set to 3 we obtained results that identified immune cell lineage. We reasoned that additional patterns could further identify biological processes in the data related to treatment. We initially tested 50 patterns, however, many of the patterns highlighted few cells, indicating an over-dimensionalization of the data. We obtained stable results when nPatterns was set to 25, with the final CoGAPS dataset stabilized at 21 patterns. Genes highly associated with each pattern were identified by calculating the PatternMarker statistic (Stein-O'Brien et al., 2017). The CalcCoGAPSStat function was used to identify pathways significantly enriched in each pattern for the MSigDB hallmark gene sets (Liberzon et al., 2015) and PanCancer Immune Profiling panel from NanoString Technologies.

Pseudotime analysis

To perform pseudotemporal ordering, the dataset was subset to relevant cell types and treatments based on the desired analysis. The root node of the trajectory was assigned by identifying the region in the UMAP dimensional reduction with low CoGAPS pattern 7 weights. Pseudotime values were assigned to cells using the order_cells function from Monocle3 version 0.2.0. Genes with significant expression changes as a function of pseudotime were identified using the graph_test function, using a multiple-testing corrected q-value cutoff of 0.01.

Linear modeling

TCGA expression and metadata were aggregated using the R/Bioconductor package TCGAbiolinks version 2.14.1 (Colaprico et al., 2016), and was used as input for transfer learning as described below. Samples were restricted to those that were labeled as "Primary solid tumor" (n=9113), "Recurrent solid tumor" (n=46), and "Metastatic" (n=394) in the "definition" column of the TCGA metadata, which resulted in 9,553 total samples. Measures of overall survival and age at diagnosis for TCGA samples were taken from those aggregated by Liu et al. (Liu et al., 2018). After scaling and centering the data, linear models were run according to the following equation:

$$OS - C + P_i \ldots P_n + A$$

Where OS equals overall survival, C represents cancer type as a categorical variable, $P_i \ldots P_n$ represent each transcriptional signature, or pattern, as separate continuous covariates, and A equals age at diagnosis. Linear models fit per cancer type were run on samples belonging to each respective cancer, and did not include the cancer type covariate C from the equation above. Models looking at the relationship between age and patterns replaced OS in the equation above with A.

Survival analysis

Kaplan Meyer plots were generated in R using the survfit function from the survival package version 3.1-12, and the ggsurvplot function from the survminer package version 0.4.6. Samples were split into those in the top 5% of pattern 7 scores, and those in the bottom 95% (i.e. all other samples).

Correlation analysis

To compare the expression of CTLA-4 and CIBERSORT scores for various immune cell types across immunogenic solid tumors from TCGA, we calculated the Spearman correlation coefficients using the cor.test function in R. For correlations between the expression of B7 (CD80, CD86) in SKCM tumors and pattern 7 weight, we used Pearson's product moment correlation as implemented in the cor.test function in R.

Transfer learning

To examine whether the mouse patterns corresponded to similar immunotherapy responses in human data, we used The R/Bioconductor package projectR (Sharma et al., 2019b) version 1.0.0 to project the expression matrix from several datasets into the CoGAPS pattern amplitude matrix (Stein-O'Brien et al., 2019). The CoGAPS result object and the expression matrix from a human dataset is used as input to the projectR function. This algorithm returns a new pattern matrix, which estimates the role of each pattern in each cell of the human dataset. This comparison of pattern across species usage enabled us to determine how each pattern defines features present in the human dataset (i.e. cell types and immune cell activation). Homologous genes present in the mouse and human data were retained for projection. Genes without homologs in the human data were removed.

Pattern performance of predicting anti-CTLA-4 response

The projected pattern weights is a continuous range of values, instead of a binary outcome. Using the individual projected pattern weight for each cell and a binary response outcome to anti-CTLA-4, we performed ROC curve analysis using the ROCR package, version 1.0-7 to determine the true-positive rates versus false-positive rates of pattern 7 weights to classify response. The area under the ROC curve was used as the quality metric to determine the prediction performance.

Cell lines and materials

All human NK cell lines (NK-92, NK-92-CD16v, NKL, YT, and KHYG-1) were kindly provided by Dr. Kerry S. Campbell (Fox Chase Cancer Center, Philadelphia, PA). The NK-92-CD16v expressed GFP due to transduction with pBMN-IRES-EGFP containing the FcRIIIA construct. All NK cell lines were cultured as previously described (Aldeghaither et al., 2019). Fresh healthy donor NK cells were purchased from AllCells (PB012-P). These NK cells were positively selected from donor peripheral blood using CD56 positivity. Donor NK cell purity was 98-99%. CTLA-4 overexpressing Jurkat cell line was generated using lentiviral transduction purchased from GP Blosciences (Product ID: LYV-CTLA4, SKU: LTV0710) which contained full length human CTLA4 gene subcloned into lentiviral expression vector pLTC with an upstream CMV promoter with puromycin selection marker. Jurkat cells were transduced using millipore sigma's spinoculation protocol. In brief, lentiviral particle solution was added to 2 X 106 Jurkat cells at a final multiplicity of infection of 1, 5 and 10. Cells were centrifuged at 800 xg for 30 minutes at 32°C then resuspended in complete growth medium for 3 days. After three days, cells were resuspended in complete medium containing 5 ug/mL puromycin overnight for selection. Selection was performed twice.

qRT-PCR

RNA was isolated using the PureLink RNA Mini Kit (Ambion). The RNA concentration was measured using NanoDrop 8000 (Thermo Fisher Scientific). cDNA was generated from 20-100 ng of RNA using the GoTaq 2-step RT-qPCR System (Promega). qPCR was performed with SYBR Green on a StepOnePlus real-time PCR system (Applied Biosystems). Gene expression was normalized to HPRT and analyzed using 1/DCt method with triplicates.

Primers used were:

CTLA-4: (F: CATGATGGGGAATGAGTTGACC; R: TCAGTCCTTGGATAGTGAGGTTC)

CD28: (F: CTATTTCCCGGACCTTCTAAGCC; R: GCGGGGAGTCATGTTCATGTA)

HPRT: (F: GATTAGCGATGATGAACCAGGTT; R: CCTCCCATCTCCTTCATGACA)

Western Blot

Cells were lysed in boiling buffer with EDTA (Boston BioProducts) supplemented with 1X protease and 1% phosphatase inhibitor prepared following the manufacturer's protocols (Sigmaaldrich, Cat.No. 11697498001 and P5726). Cleared lysate concentrations were obtained by a DC Protein Assay (BioRad). Lysates 30-50 ug were run on SDS-PAGE gels and transferred to nitrocellulose membranes (GE Healthcare). Western blots were conducted using anti-CTLA-4/CD152 (LS-C193047, LS-bio) at concentrations of 1:1000 diluted in 5% milk in PBST. Secondary antibody was anti-rabbit IgG, HRP linked (Cell Signaling) used at 1:1000. Chemiluminescent substrate (Pierce) was used for visualization.

Flow Cytometry

All cells were aliquoted into Eppendorf tubes, spun at 5000 rpm for 1 minute at 4°C, washed twice with HBSS (Fisher Scientific Cat. No. SH3058801), and resuspended in 50 L of FACS buffer (PBS plus 1% BSA) and blocked with L 1 human Fc block (BD Biosciences, 564219) for 20 minutes at 4°C. Labeled antibodies were then added at the manufacturer's recommended

concentrations and incubated at 4°C for 30 minutes, with vortexing at 15 minutes. Cells were then washed with FACS buffer twice and resuspended in FACS buffer or fixative (1% PFA in PBS). Flow antibodies included anti-human CD152 (CTLA-4) (BD Bioscience 555853) and CD28 (Biolegend 302907). The CD152 antibody has previously been shown to adequately detect CTLA-4 expression on both human T and B cells (29). Samples were run in the Georgetown Lombardi Comprehensive Cancer Center Flow Cytometry Cell Sorting Shared Resource using BD LSRFortessa. Analyses were performed using FlowJo (v10.4.1).

Immunofluorescence

Ipilimumab was acquired from the Medstar Georgetown University Hospital. Ipilimumab was labelled with Dylight550 fluorophore using the Dylight550 Conjugation Kit (Fast)- LightningLink (abcam, ab201800). In short, Ipilimumab was diluted from 5 mg/mL to 2 mg/mL using sterile PBS. Human IgG (Jackson ImmunoResearch, 009-000-003) was diluted from 11mg/mL to 2 mg/mL using sterile PBS. 1 uL of modifying reagent was added to 10 uL diluted ipilimumab and 10 uL diluted human IgG. 10 uL antibody was then added to the conjugation mix and incubated at room temperature in the dark for approximately 6 hours. 1 uL of quencher reagent was added to the labeled ipilimumab and the antibody was stored in the dark at 4°C. NK-92 and PANC-1 cells were collected and washed with cold PBS and brought to a final concentration of 1 X 106 cells/mL in staining buffer (1% BSA in PBS) in 50 uL. 50 uL of labelled ipilimumab or human IgG was added to cells to yield a final concentration of 1 ug/mL antibody. Cells were incubated in the dark at 4°C for 1 hour. After incubation, cells were pelleted and washed three times with cold PBS. Cells were brought to a final concentration of 0.5 X 106 cells/mL and 100 uL was immobilized on slides using cytospin (Cytospin 2, Shandon) for 5 mins at 1000 rpm. Following immobilization cells were fixed with 4% PFA for 10 minutes at room temperature then washed three times with cold PBS. Coverslips were mounted using VectraSheild mounting media with DAPI and sealed using clear nailpolish and allowed to dry overnight in the dark. Analyses were performed with the Leica SP8 AOBS laser scanning confocal microscope.

TCGA and CCLE expression analysis

CD86 expression was assessed in TCGA tumor samples versus paired normal controls using GEPIA: a web server for cancer and normal gene expression profiling and interactive analyses (Tang et al., 2017). CD86 expression in cancer cell lines was assessed using cbiobortal (Cerami et al., 2012; Gao et al., 2013) to analyze data from the cancer cell line encyclopedia (Barretina et al., 2012).

Software availability

All code used for this analysis is available at:

https://github.com/edavis71/projectR_ICI

Acknowledgments

This work was supported by grants from the NIH (R01CA177669, U01CA196390, and U01CA212007 to EJF) and AWS cloud credits for education. EMJ acknowledges funding from the Broccoli Foundation, The Bloomberg Kimmel Institute for Cancer Immunotherapy, and The Skip Viragh Center for Pancreas Cancer Clinical Research and Patient Care, and The Commonwealth Foundation for Cancer Research. EMJ is also supported through NIH R01CA184926, as well as Stand Up To Cancer which is a program of the Entertainment Industry Foundation administered by the American Association for Cancer Research. EJF and EMJ are also supported through the NIH P50CA062924 and P30CA006973, the Lustgarten Foundation, the Allegheny Health Network, and the Emerson Foundation (640183). LVD is supported through P30CA006973 and R50CA243627. LMW is also supported through NIH CA50633 and CA51008. AAF is supported through NIH F30 CA239441. We thank Dr. Kerry Campbell for providing the NK cell lines and Dr. Todd Armstrong, Dr. Kerry Campbell, Dr. Luciane Kagohara, Dr. Sandra Jablonski and Dr. Jackie Zimmerman for feedback on the manuscript. Figures 1A and 7G were created with Biorender.com.

References

1. Alvarez-Breckenridge, C.A., Yu, J., Kaur, B., Caligiuri, M.A., and Chiocca, E.A. (2012). Deciphering the Multifaceted Relationship between Oncolytic Viruses and Natural Killer Cells. Adv. Virol. 2012, 702839.
2. de Andrade, L.F., Lu, Y., Luoma, A., Ito, Y., Pan, D., Pyrdol, J.W., Yoon, C.H., Yuan, G.-C., and Wucherpfennig, K.W. (2019). Discovery of specialized NK cell populations infiltrating human melanoma metastases. JCI Insight 4.
3. Azuma, M., Cayabyab, M., Buck, D., Phillips, J.H., and Lanier, L.L. (1992). Involvement of CD28 in MHC-unrestricted cytotoxicity mediated by a human natural killer leukemia cell line. J. Immunol. 149, 1115–1123.
4. Barretina, J., Caponigro, G., Stransky, N., Venkatesan, K., Margolin, A.A., Kim, S., Wilson, C.J., Lehár, J., Kryukov, G.V., Sonkin, D., et al. (2012). The Cancer Cell Line Encyclopedia enables predictive modelling of anticancer drug sensitivity. Nature 483, 603–607.
5. Barry, K.C., Hsu, J., Broz, M.L., Cueto, F.J., Binnewies, M., Combes, A.J., Nelson, A.E., Loo, K., Kumar, R., Rosenblum, M.D., et al. (2018). A natural killer-dendritic cell axis defines checkpoint therapy-responsive tumor microenvironments. Nat. Med. 24, 1178–1191.
6. Brown, C.C., Gudjonson, H., Pritykin, Y., Deep, D., Lavallée, V.-P., Mendoza, A., Fromme, R., Mazutis, L., Ariyan, C., Leslie, C., et al. (2019). Transcriptional Basis of Mouse and Human Dendritic Cell Heterogeneity. Cell 179, 846–863.e24.
7. Cancer Genome Atlas Research Network, Weinstein, J.N., Collisson, E.A., Mills, G.B., Shaw, K.R.M., Ozenberger, B.A., Ellrott, K., Shmulevich, I., Sander, C., and Stuart, J.M. (2013). The Cancer Genome Atlas Pan-Cancer analysis project. Nat. Genet. 45, 1113–1120.
8. Cerami, E., Gao, J., Dogrusoz, U., Gross, B.E., Sumer, S.O., Aksoy, B.A., Jacobsen, A., Byrne, C.J., Heuer, M.L., Larsson, E., et al. (2012). The cBio cancer genomics portal: an open platform for exploring multidimensional cancer genomics data. Cancer Discov. 2, 401–404.
9. Chambers, B.J., Salcedo, M., and Ljunggren, H.G. (1996). Triggering of natural killer cells by the costimulatory molecule CD80 (B7-1). Immunity 5, 311–317.
10. Chambers, C.A., Kuhns, M.S., Egen, J.G., and Allison, J.P. (2001). CTLA-4-mediated inhibition in regulation of T cell responses: mechanisms and manipulation in tumor immunotherapy. Annu. Rev. Immunol. 19, 565–594.
11. Chen, G., Ning, B., and Shi, T. (2019). Single-Cell RNA-Seq Technologies and Related Computational Data Analysis. Front. Genet. 10, 317.
12. Colaprico, A., Silva, T.C., Olsen, C., Garofano, L., Cava, C., Garolini, D., Sabedot, T.S., Malta, T.M., Pagnotta, S.M., Castiglioni, I., et al. (2016). TCGAbiolinks: an R/Bioconductor package for integrative analysis of TCGA data. Nucleic Acids Res. 44, e71.
13. Concha-Benavente, F., Kansy, B., Moskovitz, J., Moy, J., Chandran, U., and Ferris, R.L. (2018). PD-L1 Mediates Dysfunction in Activated PD-1+ NK Cells in Head and Neck Cancer Patients. Cancer Immunol Res 6, 1548–1560.
14. Contardi, E., Palmisano, G.L., Tazzari, P.L., Martelli, A.M., Falà, F., Fabbi, M., Kato, T., Lucarelli, E., Donati, D., Polito, L., et al. (2005). CTLA-4 is constitutively expressed on tumor cells and can trigger apoptosis upon ligand interaction. Int. J. Cancer 117, 538–550.
15. Crinier, A., Milpied, P., Escalière, B., Piperoglou, C., Galluso, J., Balsamo, A., Spinelli, L., Cervera-Marzal, I., Ebbo, M., Girard-Madoux, M., et al. (2018). High-Dimensional Single-Cell Analysis Identifies Organ-Specific Signatures and Conserved NK Cell Subsets in Humans and Mice. Immunity 49, 971–986.e5.

16. Cursons, J., Souza-Fonseca-Guimaraes, F., Foroutan, M., Anderson, A., Hollande, F., Hediyeh-Zadeh, S., Behren, A., Huntington, N.D., and Davis, M.J. (2019). A Gene Signature Predicting Natural Killer Cell Infiltration and Improved Survival in Melanoma Patients. Cancer Immunol Res 7, 1162–1174.
17. Dammeijer, F., Lau, S.P., van Eijck, C.H.J., van der Burg, S.H., and Aerts, J.G.J.V. (2017). Rationally combining immunotherapies to improve efficacy of immune checkpoint blockade in solid tumors. Cytokine Growth Factor Rev. 36, 5–15.
18. Darlington, P.J., Kirchhof, M.G., Criado, G., Sondhi, J., and Madrenas, J. (2005). Hierarchical regulation of CTLA-4 dimer-based lattice formation and its biological relevance for T cell inactivation. J. Immunol. 175, 996–1004.
19. Du, X., Tang, F., Liu, M., Su, J., Zhang, Y., Wu, W., Devenport, M., Lazarski, C.A., Zhang, P., Wang, X., et al. (2018). A reappraisal of CTLA-4 checkpoint blockade in cancer immunotherapy. Cell Res. 28, 416–432.
20. Esposito, L., Hunter, K.M.D., Clark, J., Rainbow, D.B., Stevens, H., Denesha, J., Duley, S., Dawson, S., Coleman, G., Nutland, S., et al. (2014). Investigation of soluble and transmembrane CTLA-4 isoforms in serum and microvesicles. J. Immunol. 193, 889–900.
21. Ferrara, R., Susini, S., and Marabelle, A. (2019). Anti-CTLA-4 Immunotherapy Does Not Deplete FOXP3+ Regulatory T Cells (Tregs) in Human Cancers-Letter. Clin. Cancer Res. 25, 3468.
22. Galea-Lauri, J., Darling, D., Gan, S.U., Krivochtchapov, L., Kuiper, M., Gäken, J., Souberbielle, B., and Farzaneh, F. (1999). Expression of a variant of CD28 on a subpopulation of human NK cells: implications for B7-mediated stimulation of NK cells. J. Immunol. 163, 62–70.
23. Gao, J., Aksoy, B.A., Dogrusoz, U., Dresdner, G., Gross, B., Sumer, S.O., Sun, Y., Jacobsen, A., Sinha, R., Larsson, E., et al. (2013). Integrative analysis of complex cancer genomics and clinical profiles using the cBioPortal. Sci. Signal. 6, l1.
24. Gotthardt, D., and Sexl, V. (2016). STATs in NK-Cells: The Good, the Bad, and the Ugly. Front. Immunol. 7, 694.
25. Gubin, M.M., Esaulova, E., Ward, J.P., Malkova, O.N., Runci, D., Wong, P., Noguchi, T., Arthur, C.D., Meng, W., Alspach, E., et al. (2018). High-Dimensional Analysis Delineates Myeloid and Lymphoid Compartment Remodeling during Successful Immune-Checkpoint Cancer Therapy. Cell 175, 1014–1030.e19.
26. Hodi, F.S., O'Day, S.J., McDermott, D.F., Weber, R.W., Sosman, J.A., Haanen, J.B., Gonzalez, R., Robert, C., Schadendorf, D., Hassel, J.C., et al. (2010). Improved survival with ipilimumab in patients with metastatic melanoma. N. Engl. J. Med. 363, 711–723.
27. Hsu, J., Hodgins, J.J., Marathe, M., Nicolai, C.J., Bourgeois-Daigneault, M.-C., Trevino, T.N., Azimi, C.S., Scheer, A.K., Randolph, H.E., Thompson, T.W., et al. (2018). Contribution of NK cells to immunotherapy mediated by PD-1/PD-L1 blockade. J. Clin. Invest. 128, 4654–4668.
28. Jenkins, R.W., Barbie, D.A., and Flaherty, K.T. (2018). Mechanisms of resistance to immune checkpoint inhibitors. Br. J. Cancer 118, 9–16.
29. Kavanagh, B., O'Brien, S., Lee, D., Hou, Y., Weinberg, V., Rini, B., Allison, J.P., Small, E.J., and Fong, L. (2008). CTLA4 blockade expands FoxP3+ regulatory and activated effector CD4+ T cells in a dose-dependent fashion. Blood 112, 1175–1183.
30. Kim, N., and Kim, H.S. (2018). Targeting Checkpoint Receptors and Molecules for Therapeutic Modulation of Natural Killer Cells. Front. Immunol. 9, 2041.
31. Kiselev, V.Y., Andrews, T.S., and Hemberg, M. (2019). Challenges in unsupervised clustering of single-cell RNA-seq data. Nat. Rev. Genet. 20, 273–282.
32. Kohlhapp, F.J., Broucek, J.R., Hughes, T., Huelsmann, E.J., Lusciks, J., Zayas, J.P., Dolubizno, H., Fleetwood, V.A., Grin, A., Hill, G.E., et al. (2015). NK cells and CD8+ T cells cooperate to improve therapeutic responses in melanoma treated with interleukin-2 (IL-2) and CTLA-4 blockade. J Immunother Cancer 3, 18.
33. Kotliar, D., Veres, A., Nagy, M.A., Tabrizi, S., Hodis, E., Melton, D.A., and Sabeti, P.C. (2019). Identifying gene expression programs of cell-type identity and cellular activity with single-cell RNA-Seq. Elife 8.
34. Krummel, M.F., and Allison, J.P. (1996). CTLA-4 engagement inhibits IL-2 accumulation and cell cycle progression upon activation of resting T cells. J. Exp. Med. 183, 2533–2540.
35. Lang, S., Vujanovic, N.L., Wollenberg, B., and Whiteside, T.L. (1998). Absence of B7.1-CD28/CTLA-4-mediated co-stimulation in human NK cells. Eur. J. Immunol. 28, 780–786. Lanier, L.L. (2000). Turning on natural killer cells. J. Exp. Med. 191, 1259–1262.
36. Larkin, J., Chiarion-Sileni, V., Gonzalez, R., Grob, J.J., Cowey, C.L., Lao, C.D., Schadendorf, D., Dummer, R., Smylie, M., Rutkowski, P., et al. (2015). Combined Nivolumab and Ipilimumab or Monotherapy in Untreated Melanoma. N. Engl. J. Med. 373, 23–34.
37. Li, J., Yang, Y., Inoue, H., Mori, M., and Akiyoshi, T. (1996). The expression of costimulatory molecules CD80 and CD86 in human carcinoma cell lines: its regulation by interferon gamma and interleukin-10. Cancer Immunol. Immunother. 43, 213–219.
38. Liberzon, A., Birger, C., Thorvaldsdóttir, H., Ghandi, M., Mesirov, J.P., and Tamayo, P. (2015). The Molecular Signatures Database (MSigDB) hallmark gene set collection. Cell Syst 1, 417–425.
39. Liu, J., Lichtenberg, T., Hoadley, K.A., Poisson, L.M., Lazar, A.J., Cherniack, A.D., Kovatich, A.J., Benz, C.C., Levine, D.A., Lee, A.V., et al. (2018). An Integrated TCGA Pan-Cancer Clinical Data Resource to Drive High-Quality Survival Outcome Analytics. Cell 173, 400–416.e11.
40. López-Soto, A., Gonzalez, S., Smyth, M.J., and Galluzzi, L. (2017). Control of Metastasis by NK Cells. Cancer Cell 32, 135–154.
41. Lu, D., Ni, Z., Liu, X., Feng, S., Dong, X., Shi, X., Zhai, J., Mai, S., Jiang, J., Wang, Z., et al. (2019). Beyond T Cells: Understanding the Role of PD-1/PD-L1 in Tumor-Associated Macrophages. J Immunol Res 2019, 1919082.
42. Luque, I., Reyburn, H., and Strominger, J.L. (2000). Expression of the CD80 and CD86 molecules enhances cytotoxicity by human natural killer cells. Hum. Immunol. 61, 721–728.
43. Marchiori, C., Scarpa, M., Kotsafti, A., Morgan, S., Fassan, M., Guzzardo, V., Porzionato, A., Angriman, I., Ruffolo, C., Sut, S., et al. (2019). Epithelial CD80 promotes immune surveillance of colonic preneoplastic lesions and its expression is increased by oxidative stress through STAT3 in colon cancer cells. J. Exp. Clin. Cancer Res. 38, 190.
44. Mariotti, F.R., Petrini, S., Ingegnere, T., Tumino, N., Besi, F., Scordamaglia, F., Munari, E., Pesce, S., Marcenaro, E., Moretta, A., et al. (2019). PD-1 in human NK cells: evidence of cytoplasmic mRNA and protein expression. Oncoimmunology 8, 1557030.
45. Martín-Fontecha, A., Assarsson, E., Carbone, E., Kärre, K., and Ljunggren, H.G. (1999). Triggering of murine NK cells by CD40 and CD86 (B7-2). J. Immunol. 162, 5910–5916. McInnes, L., Healy, J., and Melville, J. (2018). UMAP: Uniform Manifold Approximation and Projection for Dimension Reduction.
46. Motzer, R.J., Tannir, N.M., McDermott, D.F., Arén Frontera, O., Melichar, B., Choueiri, T.K., Plimack, E.R., Barthélémy, P., Porta, C., George, S., et al. (2018). Nivolumab plus Ipilimumab versus Sunitinib in Advanced Renal-Cell Carcinoma. N. Engl. J. Med. 378, 1277–1290.
47. Newman, A.M., Liu, C.L., Green, M.R., Gentles, A.J., Feng, W., Xu, Y., Hoang, C.D., Diehn, M., and Alizadeh, A.A. (2015). Robust enumeration of cell subsets from tissue expression profiles. Nat. Methods 12, 453–457.
48. Overman, M.J., Lonardi, S., Wong, K.Y.M., Lenz, H.-J., Gelsomino, F., Aglietta, M., Morse, M.A., Van Cutsem, E., McDermott, R., Hill, A., et al. (2018). Durable Clinical Benefit With Nivolumab Plus Ipilimumab in DNA Mismatch Repair-Deficient/Microsatellite Instability-High Metastatic Colorectal Cancer. J. Clin. Oncol. 36, 773–779.
49. Passariello, M., Camorani, S., Vetrei, C., Ricci, S., Cerchia, L., and De Lorenzo, C. (2020). Ipilimumab and Its Derived EGFR Aptamer-Based Conjugate Induce Efficient NK Cell Activation against Cancer Cells. Cancers 12.
50. Patil, V.S., Madrigal, A., Schmiedel, B.J., Clarke, J., O'Rourke, P., de Silva, A.D., Harris, E., Peters, B., Seumois, G., Weiskopf, D., et al. (2018). Precursors of human CD4+ cytotoxic T lymphocytes identified by single-cell transcriptome analysis. Sci Immunol 3.
51. Perel, P., Roberts, I., Sena, E., Wheble, P., Briscoe, C., Sandercock, P., Macleod, M., Mignini, L.E., Jayaram, P., and Khan, K.S. (2007). Comparison of treatment effects between animal experiments and clinical trials: systematic review. BMJ 334, 197.
52. Pistillo, M.P., Tazzari, P.L., Palmisano, G.L., Pierri, I., Bolognesi, A., Ferlito, F., Capanni, P., Polito, L., Ratta, M., Pileri, S., et al. (2003). CTLA-4 is not restricted to the lymphoid cell lineage and can function as a target molecule for apoptosis induction of leukemic cells. Blood 101, 202–209.
53. Puram, S.V., Tirosh, I., Parikh, A.S., Patel, A.P., Yizhak, K., Gillespie, S., Rodman, C., Luo, C.L., Mroz, E.A., Emerick, K.S., et al. (2017). Single-Cell Transcriptomic Analysis of Primary and Metastatic Tumor Ecosystems in Head and Neck Cancer. Cell 171, 1611–1624.e24.
54. Quezada, S.A., Peggs, K.S., Curran, M.A., and Allison, J.P. (2006). CTLA4 blockade and GM-CSF combination immunotherapy alters the intratumor balance of effector and regulatory T cells. J. Clin. Invest. 116, 1935–1945.
55. Robert, C., Thomas, L., Bondarenko, I., O'Day, S., Weber, J., Garbe, C., Lebbe, C., Baurain, J.-F., Testori, A., Grob, J.-J., et al. (2011). Ipilimumab plus dacarbazine for previously untreated metastatic melanoma. N. Engl. J. Med. 364, 2517–2526.
56. Rodig, S.J., Gusenleitner, D., Jackson, D.G., Gjini, E., Giobbie-Hurder, A., Jin, C., Chang, H., Lovitch, S.B., Horak, C., Weber, J.S., et al. (2018). MHC proteins confer differential sensitivity to CTLA-4 and PD-1 blockade in untreated metastatic melanoma. Sci. Transl. Med. 10.
57. Rowshanravan, B., Halliday, N., and Sansom, D.M. (2018). CTLA-4: a moving target in immunotherapy. Blood 131, 58–67.
58. Sade-Feldman, M., Jiao, Y.J., Chen, J.H., Rooney, M.S., Barzily-Rokni, M., Eliane, J.-P., Bjorgaard, S.L., Hammond, M.R., Vitzthum, H., Blackmon, S.M., et al. (2017). Resistance to checkpoint blockade therapy through inactivation of antigen presentation. Nat. Commun. 8, 1136.
59. Sade-Feldman, M., Yizhak, K., Bjorgaard, S.L., Ray, J.P., de Boer, C.G., Jenkins, R.W., Lieb, D.J., Chen, J.H., Frederick, D.T., Barzily-Rokni, M., et al. (2018). Defining T Cell States Associated with Response to Checkpoint Immunotherapy in Melanoma. Cell 175, 998–1013.e20.
60. Sanseviero, E., O'Brien, E.M., Karras, J.R., Shabaneh, T.B., Aksoy, B.A., Xu, W., Zheng, C., Yin, X., Xu, X., Karakousis, G.C., et al. (2019). Anti-CTLA-4 Activates Intratumoral NK Cells and Combined with IL15/IL15R Complexes Enhances Tumor Control. Cancer Immunol Res 7, 1371–1380.
61. Schmidt, E.M., Wang, C.J., Ryan, G.A., Clough, L.E., Qureshi, O.S., Goodall, M., Abbas, A.K., Sharpe, A.H., Sansom, D.M., and Walker, L.S.K. (2009). Ctla-4 controls regulatory T cell peripheral homeostasis and is required for suppression of pancreatic islet autoimmunity. J. Immunol. 182, 274–282.
62. Sharma, A., Subudhi, S.K., Blando, J., Scutti, J., Vence, L., Wargo, J., Allison, J.P., Ribas, A., and Sharma, P. (2019a). Anti-CTLA-4 Immunotherapy Does Not Deplete FOXP3+ Regulatory T Cells (Tregs) in Human Cancers. Clin. Cancer Res. 25, 1233–1238.

63. Sharma, G., Colantuoni, C., Goff, L.A., Fertig, E.J., and Stein-O'Brien, G. (2019b). projectR: An R/Bioconductor package for transfer learning via PCA, NMF, correlation, and clustering.
64. Shimasaki, N., Jain, A., and Campana, D. (2020). NK cells for cancer immunotherapy. Nat. Rev. Drug Discov. 19, 200–218.
65. Simmons, D., and Seed, B. (1988). The Fc gamma receptor of natural killer cells is a phospholipid-linked membrane protein. Nature 333, 568–570.
66. Simpson, T.R., Li, F., Montalvo-Ortiz, W., Sepulveda, M.A., Bergerhoff, K., Arce, F., Roddie, C., Henry, J.Y., Yagita, H., Wolchok, J.D., et al. (2013). Fc-dependent depletion of tumor-infiltrating regulatory T cells co-defines the efficacy of anti-CTLA-4 therapy against melanoma. J. Exp. Med. 210, 1695–1710.
67. Smith, S.L., Kennedy, P.R., Stacey, K.B., Worboys, J.D., Yarwood, A., Seo, S., Solloa, E.H., Mistretta, B., Chatterjee, S.S., Gunaratne, P., et al. (2020). Diversity of peripheral blood human NK cells identified by single-cell RNA sequencing. Blood Adv 4, 1388–1406.
68. Stein-O'Brien, G.L., Carey, J.L., Lee, W.S., Considine, M., Favorov, A.V., Flam, E., Guo, T., Li, S., Marchionni, L., Sherman, T., et al. (2017). PatternMarkers GWCoGAPS for novel data-driven biomarkers via whole transcriptome NMF. Bioinformatics 33, 1892–1894.
69. Stein-O'Brien, G.L., Arora, R., Culhane, A.C., Favorov, A.V., Garmire, L.X., Greene, C.S., Goff, L.A., Li, Y., Ngom, A., Ochs, M.F., et al. (2018). Enter the Matrix: Factorization Uncovers Knowledge from Omics. Trends Genet. 34, 790–805.
70. Stein-O'Brien, G.L., Clark, B.S., Sherman, T., Zibetti, C., Hu, Q., Sealfon, R., Liu, S., Qian, J., Colantuoni, C., Blackshaw, S., et al. (2019). Decomposing Cell Identity for Transfer Learning across Cellular Measurements, Platforms, Tissues, and Species. Cell Syst 8, 395–411.e8.
71. Stojanovic, A., Fiegler, N., Brunner-Weinzierl, M., and Cerwenka, A. (2014). CTLA-4 is expressed by activated mouse NK cells and inhibits NK Cell IFN- production in response to mature dendritic cells. J. Immunol. 192, 4184–4191.
72. Sutmuller, R.P., van Duivenvoorde, L.M., van Elsas, A., Schumacher, T.N., Wildenberg, M.E., Allison, J.P., Toes, R.E., Offringa, R., and Melief, C.J. (2001). Synergism of cytotoxic T lymphocyte-associated antigen 4 blockade and depletion of CD25(+) regulatory T cells in antitumor therapy reveals alternative pathways for suppression of autoreactive cytotoxic T lymphocyte responses. J. Exp. Med. 194, 823–832.
73. Tallerico, R., Cristiani, C.M., Staaf, E., Garofalo, C., Sottile, R., Capone, M., Pico de Coaña, Y., Madonna, G., Palella, E., Wolodarski, M., et al. (2017). IL-15, TIM-3 and NK cells subsets predict responsiveness to anti-CTLA-4 treatment in melanoma patients. Oncoimmunology 6, e1261242.
74. Tang, J., Shalabi, A., and Hubbard-Lucey, V.M. (2018). Comprehensive analysis of the clinical immuno-oncology landscape. Ann. Oncol. 29, 84–91.
75. Tang, Z., Li, C., Kang, B., Gao, G., Li, C., and Zhang, Z. (2017). GEPIA: a web server for cancer and normal gene expression profiling and interactive analyses. Nucleic Acids Res. 45, W98–W102.
76. Terrazzano, G., Zanzi, D., Palomba, C., Carbone, E., Grimaldi, S., Pisanti, S., Fontana, S., Zappacosta, S., and Ruggiero, G. (2002). Differential involvement of CD40, CD80, and major histocompatibility complex class I molecules in cytotoxicity induction and interferon-gamma production by human natural killer effectors. J. Leukoc. Biol. 72, 305–311.
77. Thorsson, V., Gibbs, D.L., Brown, S.D., Wolf, D., Bortone, D.S., Ou Yang, T.-H., Porta-Pardo, E., Gao, G.F., Plaisier, C.L., Eddy, J.A., et al. (2018). The Immune Landscape of Cancer. Immunity 48, 812–830.e14.
78. Tirapu, I., Huarte, E., Guiducci, C., Arina, A., Zaratiegui, M., Murillo, O., Gonzalez, A., Berasain, C., Berraondo, P., Fortes, P., et al. (2006). Low surface expression of B7-1 (CD80) is an immunoescape mechanism of colon carcinoma. Cancer Res. 66, 2442–2450.
79. Trapnell, C., Cacchiarelli, D., Grimsby, J., Pokharel, P., Li, S., Morse, M., Lennon, N.J., Livak, K.J., Mikkelsen, T.S., and Rinn, J.L. (2014). The dynamics and regulators of cell fate decisions are revealed by pseudotemporal ordering of single cells. Nat. Biotechnol. 32, 381–386.
80. Valk, E., Rudd, C.E., and Schneider, H. (2008). CTLA-4 trafficking and surface expression. Trends Immunol. 29, 272–279.
81. Way, G.P., Zietz, M., Rubinetti, V., Himmelstein, D.S., and Greene, C.S. (2019). Sequential compression of gene expression across dimensionalities and methods reveals no single best method or dimensionality.
82. Wilson, J.L., Charo, J., Martín-Fontecha, A., Dellabona, P., Casorati, G., Chambers, B.J., Kiessling, R., Bejarano, M.T., and Ljunggren, H.G. (1999). NK cell triggering by the human costimulatory molecules CD80 and CD86. J. Immunol. 163, 4207–4212.
83. Xiong, H., Mittman, S., Rodriguez, R., Moskalenko, M., Pacheco-Sanchez, P., Yang, Y., Nickles, D., and Cubas, R. (2019). Anti-PD-L1 Treatment Results in Functional Remodeling of the Macrophage Compartment. Cancer Res. 79, 1493–1506.
84. Yu, Z., Liao, J., Chen, Y., Zou, C., Zhang, H., Cheng, J., Liu, D., Li, T., Zhang, Q., Li, J., et al. (2019). Single-Cell Transcriptomic Map of the Human and Mouse Bladders. J. Am. Soc. Nephrol. 30, 2159–2176.
85. Zaretsky, J.M., Garcia-Diaz, A., Shin, D.S., Escuin-Ordinas, H., Hugo, W., Hu-Lieskovan, S., Torrejon, D.Y., Abril-Rodriguez, G., Sandoval, S., Barthly, L., et al. (2016). Mutations Associated with Acquired Resistance to PD-1 Blockade in Melanoma. N. Engl. J. Med. 375, 819–829.
86. Zilionis, R., Engblom, C., Pfirschke, C., Savova, V., Zemmour, D., Saatcioglu, H.D., Krishnan, I., Maroni, G., Meyerovitz, C.V., Kerwin, C.M., et al. (2019). Single-Cell Transcriptomics of Human and Mouse Lung Cancers Reveals Conserved Myeloid Populations across Individuals and Species. Immunity 50, 1317–1334.e10.

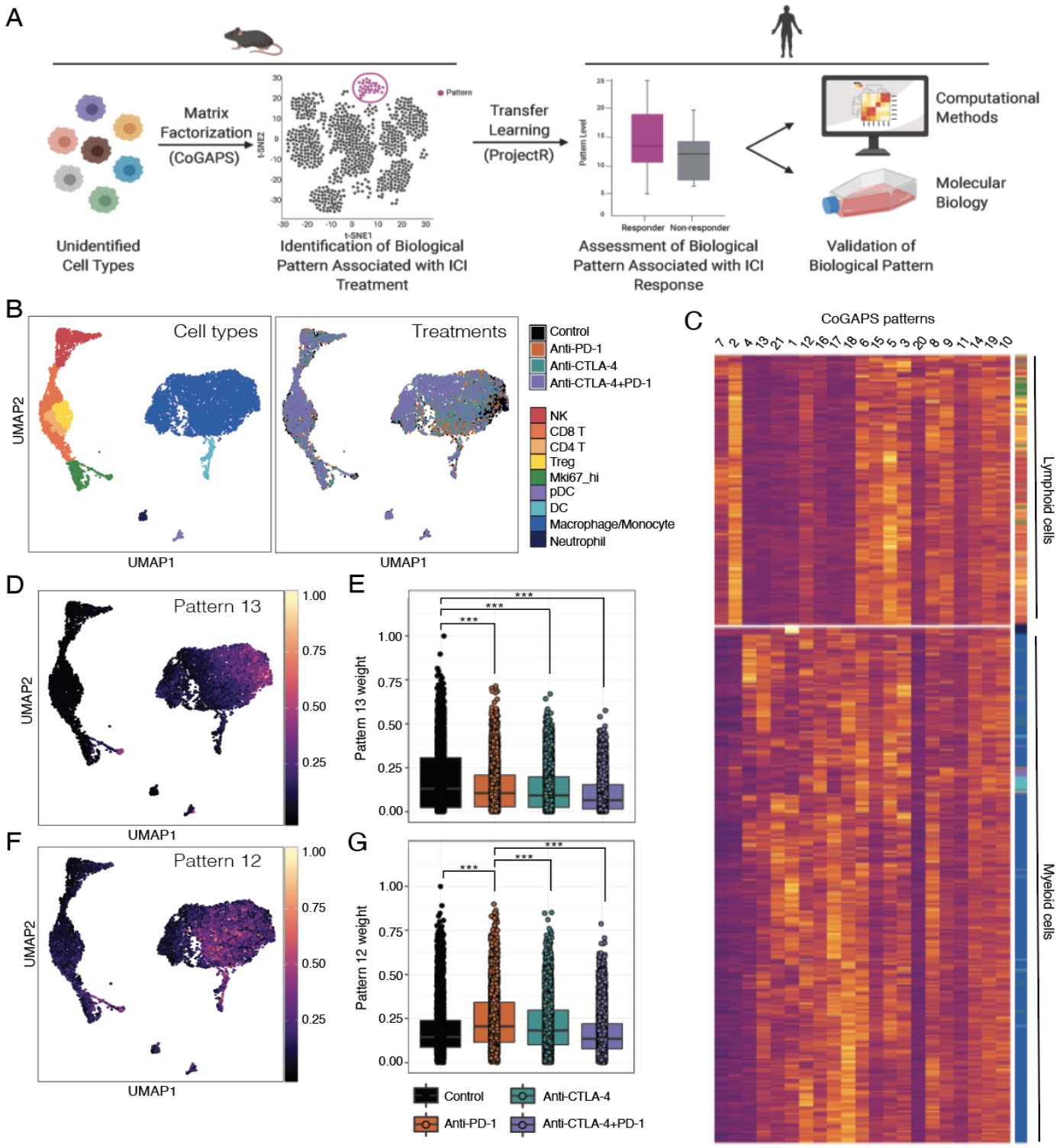

Figure 1: CoGAPS identifies gene signatures related to immune cell lineage and treatment response in mouse intratumoral immune cell scRNA-seq data. A. Schematic representation of computational pipeline. B. UMAP-dimension reduction of droplet-based scRNA-seq of intratumoral immune cells from ICI treated mouse sarcomas(Gubin et al., 2018). Samples are colored by annotated cell types (left) and by treatment (right). C. Hierarchical clustered heatmap of 21 CoGAPS pattern weights demonstrating segregation of patterns by immune cell lineage. Rows are individual cells, with column annotations designating cell type. Columns represent different CoGAPS patterns. D. UMAP-dimension reduction colored by CoGAPS pattern 13 weights illustrates a cell type specific signature within the macrophages/monocytes. E. Boxplot of pattern 13 weights in individual macrophage/monocyte cells, faceted by treatment group. Pattern 13 is associated with cells treated with control monoclonal antibody. F. UMAP-dimension reduction colored by CoGAPS pattern 12 weights illustrates a cell type specific signature within the macrophages/monocytes. G. Boxplot of pattern 12 weights in individual macrophage/monocyte cells, faceted by treatment group. Pattern 12 is associated with cells treated with anti-PD-1.

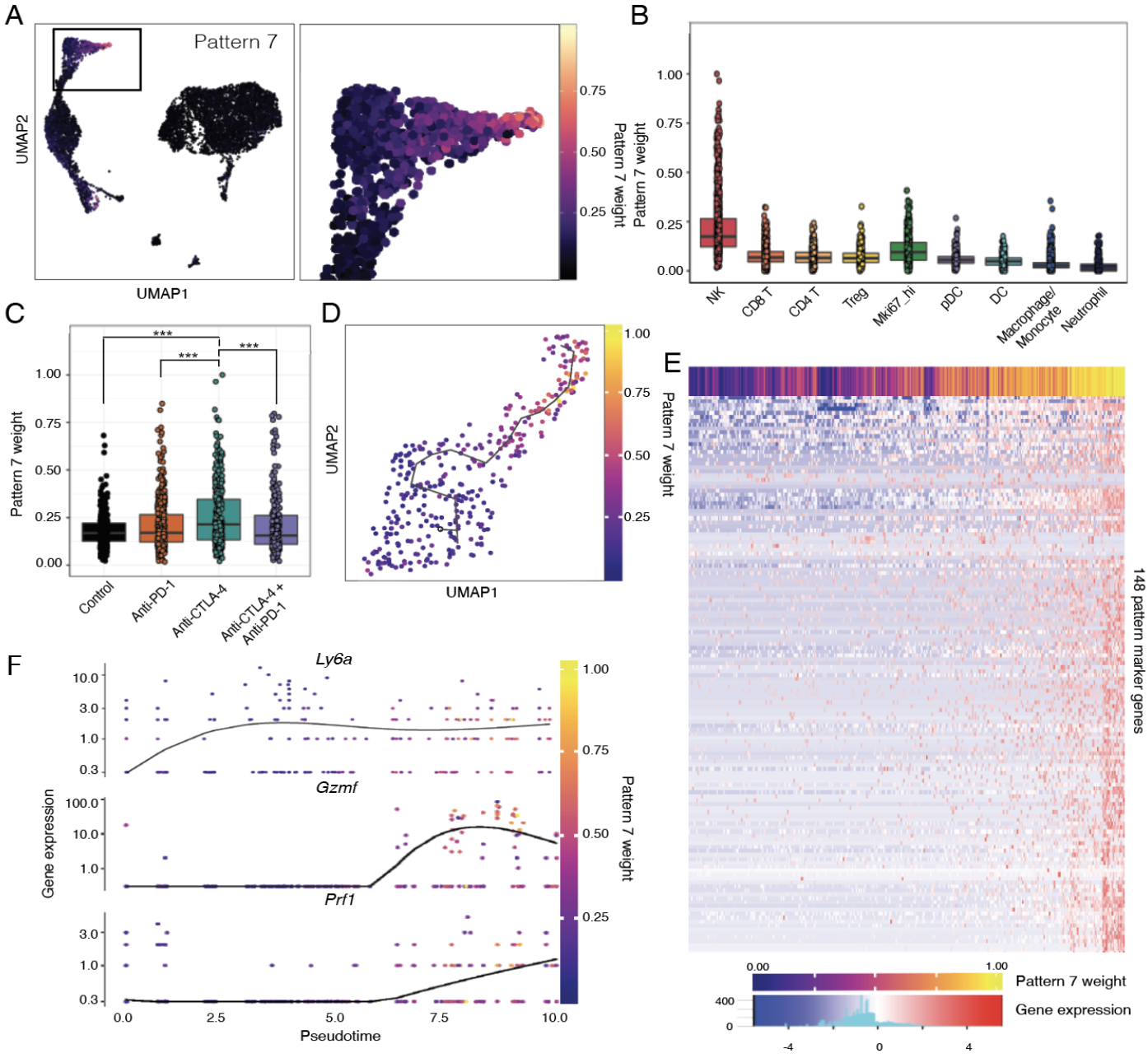

Figure 2: CoGAPS and pseudotime analysis reveals a dynamic state change in NK cells during ICI exposure in mouse scRNA-seq data. A. UMAP dimension reduction colored by CoGAPS pattern 7 weights across all cells (left) and magnified view (right) showing that pattern 7 marks a population of NK cells delineated in Fig. 1A. B. Boxplot of pattern 7 weights across each immune cell type. Cells with high pattern 7 weights are observed only in NK cells. C. Boxplot of pattern 7 weights in individual NK cells faceted by treatment group. Anti-CTLA-4 treated NK cells have increased pattern 7 weights compared to NK cells treated with other immunotherapies. D. Pseudotemporal trajectory of anti-CTLA-4 treated NK cells colored by CoGAPS pattern 7 weight suggesting that anti-CTLA-4 treatment results in NK cell activation. E. Heatmap of gene expression for 148 pattern markers that are differentially expressed across pseudotime. Columns are individual cells, and column annotation designates pattern 7 weight in each cell. Rows are differentially expressed pattern markers. F. Gene expression of selected NK cell activation associated genes differentially upregulated across pseudotime. Each dot represents a different cell and is colored by CoGAPS pattern 7 weight.

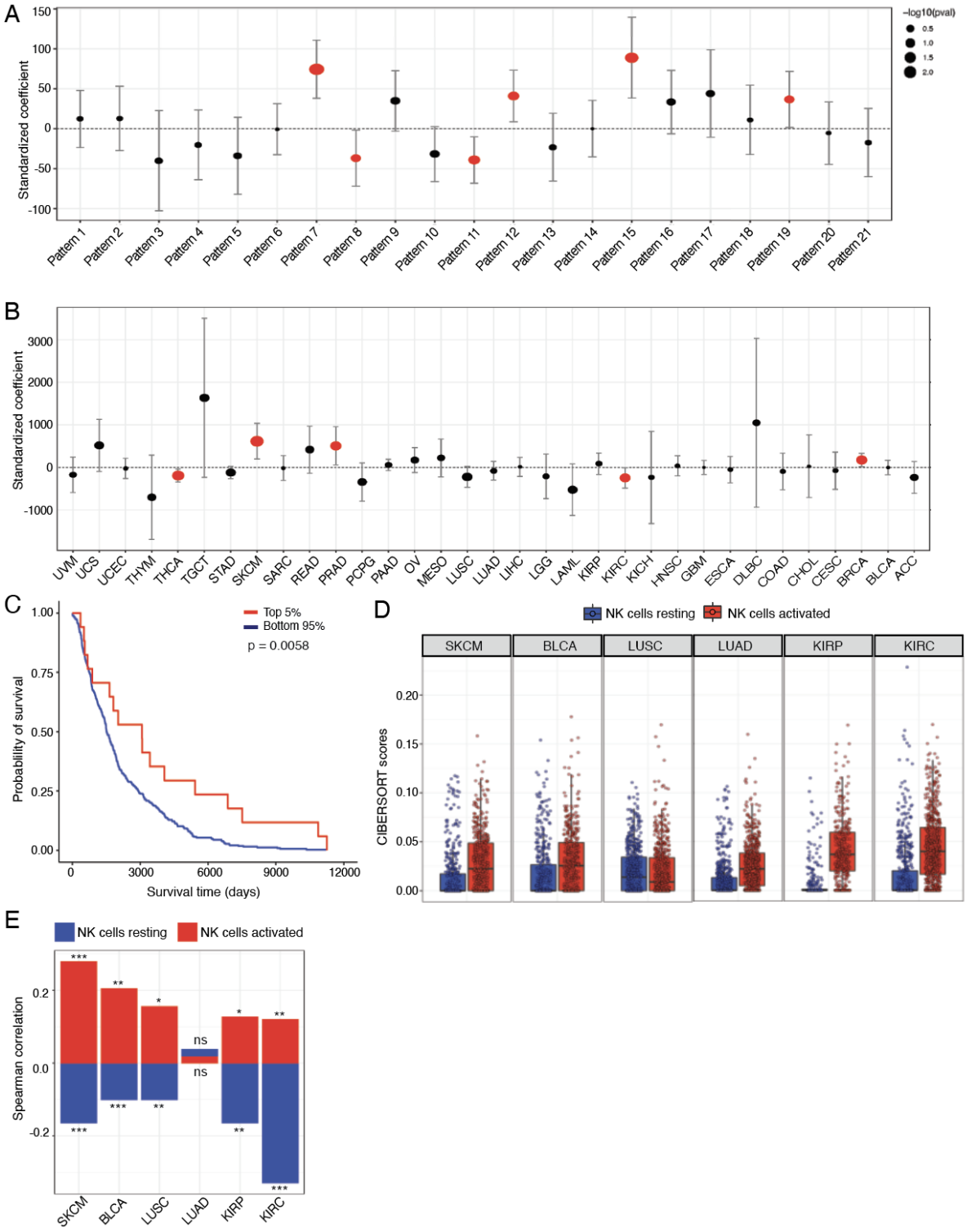

Figure 3: Preclinical NK activation signature is associated with overall survival in human melanoma. A. The output from a multiple linear regression model that predicts overall tumor survival from our transcriptional patterns, while also adjusting for cancer type as a covariate. Standardized coefficients (i.e. data was scaled and centered) representing the strength and direction of association for each pattern are shown on the x-axis, with error bars representing coefficient +- 1.96 * standard error, and point size scaled to the coefficient's p-value. Patterns 7 and 15 are most strongly positively associated with overall survival, with pattern 7 being most significantly positively associated ($p < 1.2 \times 10^{-4}$). B. The output from a multiple linear regression model that predicts overall tumor survival from our transcriptional patterns, while also adjusting for patient age as a covariate. Pattern 7 is the most significantly positively associated with overall survival in SKCM ($p < 5 \times 10^{-3}$). C. Kaplan-Meier plot of overall survival for 368 metastatic melanoma patients with the top 5D. Boxplot of CIBERSORT scores estimating the abundance of resting and activated NK cells from TCGA RNA-seq data by tumor subtype in TCGA. E. Bar plot of Spearman correlation coefficients between CTLA-4 and CIBERSORT cell type score for immunogenic cancers. CTLA-4 expression is positively correlated with estimation of activated NK cells from TCGA RNA-seq data. Significant correlations for NK scores and CTLA-4 expression are indicated by asterisks where p-values < 0.05 = *, < 0.01 = **, and p-values < 0.001 = ***.

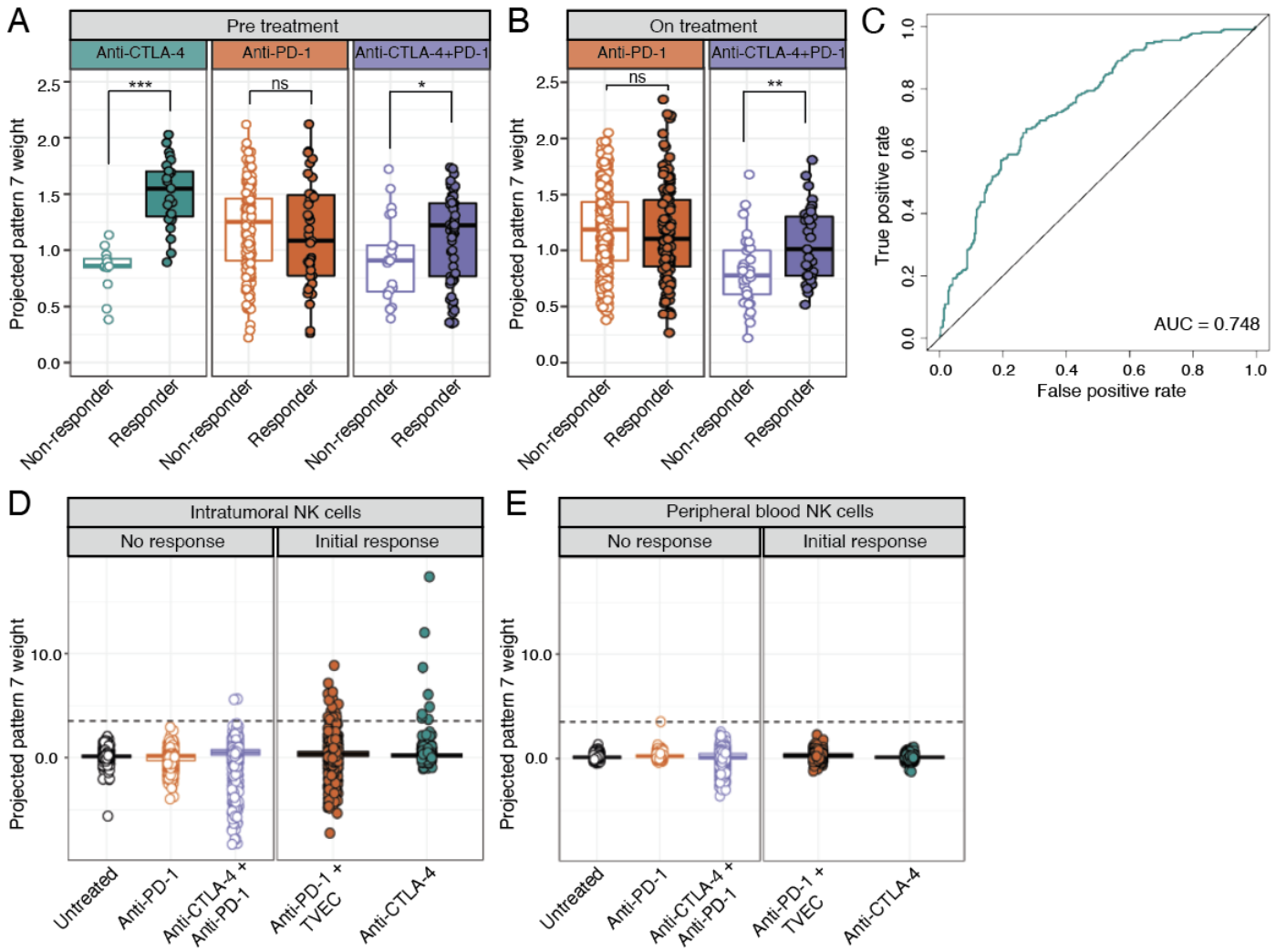

Figure 4: ProjectR recovers conserved immunotherapy response in intratumoral NK cells from independent human melanoma scRNA-seq datasets. A. Box plot of projected pattern 7 weights across intratumoral NK cells from metastatic melanoma patients prior to ICI treatment (Sade-Feldman et al., 2018). Cells are colored by therapy and separated by patient response. Increased pattern 7 is significantly associated with NK cells from patients responsive to anti-CTLA-4 or combined anti-CTLA-4 and anti-PD-1. Significant differences in mean pattern 7 weight between treatment groups are indicated by asterisks where p-values < 0.05 = *, < 0.01 = **, and p-values < 0.001 = ***. B. Box plot of projected pattern 7 weights across intratumoral NK cells from metastatic melanoma patients after treatment with ICI. Cells are colored by therapy and separated by patient response. Increased pattern 7 is associated with NK cells from patients responsive to combination anti-CTLA-4 + anti-PD-1. Significant differences in mean pattern 7 weight between treatment groups are indicated by asterisks where p-values < 0.05 = *, < 0.01 = **, and p-values < 0.001 = ***. C. ROC curve for the performance of pattern 7 weights in predicting response to anti-CTLA-4 prior to the administration of treatment. D. Box plot of projected pattern 7 weights across flow-sorted intratumoral NK cells from metastatic melanoma tumors that were unresponsive ICI (intrinsic resistance) or developed acquired resistance after a period of initial response (de Andrade et al., 2019). The dashed line indicates the average maximum value for pattern 7 across treatment groups. NK cells with elevated pattern 7 weights are seen in patients that had an initial response to ICI, with the highest observed weights from a patient that responded to anti-CTLA-4. E. Box plot of projected pattern 7 weights across NK cells isolated from peripheral blood of metastatic melanoma patients that had no response to ICI (intrinsic resistance) or developed acquired resistance after a period of initial response. The dashed line indicates the average maximum value for pattern 7 from intratumoral NK cells across treatment groups. Elevated pattern 7 weights are not detected in circulating NK cells, regardless of response.

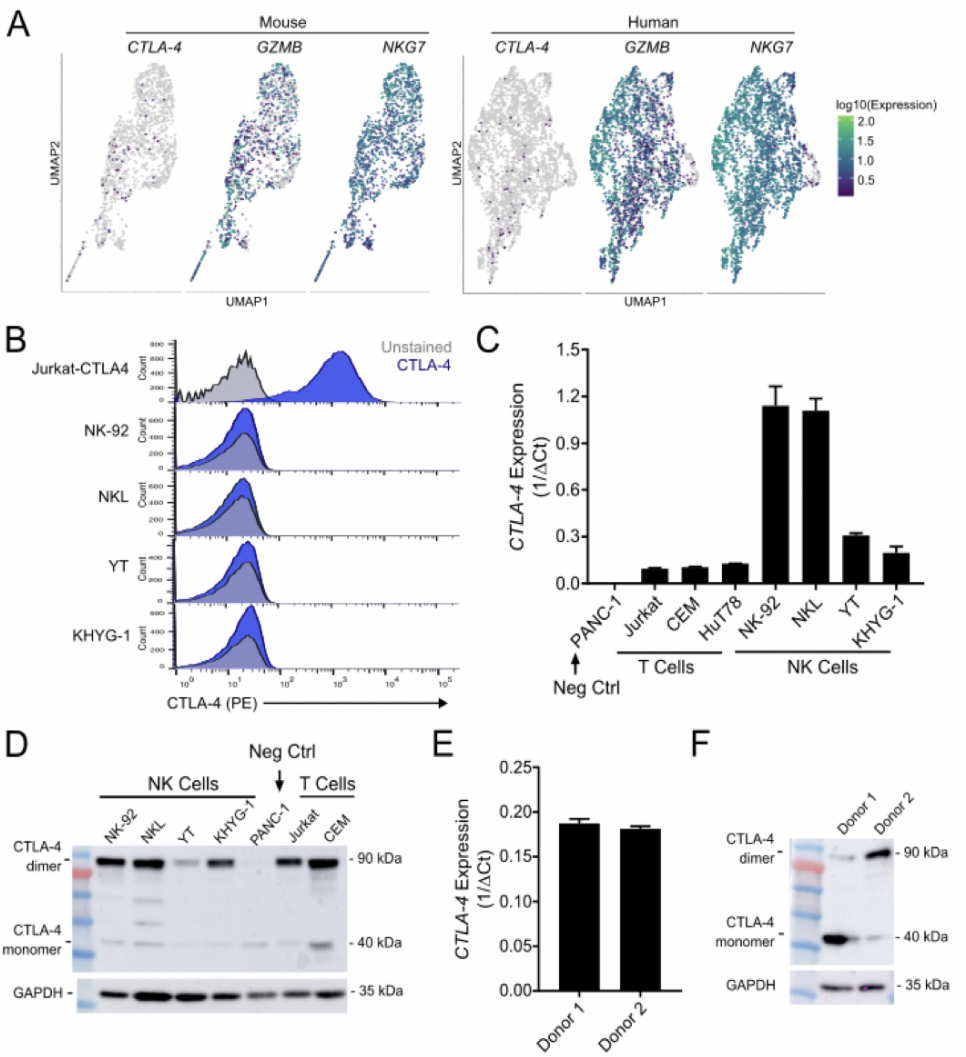

Figure 5: CTLA-4 is expressed by both human NK cell lines and healthy human donor-derived NK cells. A. UMAP dimension reduction with cells colored by single-cell gene expression for CTLA-4 and representative immune activation genes in mouse (left) and human (right) intratumoral NK cells. The pattern of CTLA-4 expression is consistent with the reduced ability of scRNA-seq to capture low to moderately expressed genes. B. Flow cytometry for surface expression of CTLA-4 in positive control (Jurkat-CTLA4) and NK cell lines (NK-92, NKL, YT, KHYG-1). C. Quantitative real-time PCR (qrt-PCR) analysis of CTLA-4 expression in a CTLA-4 null line (PANC-1), T cell lines (Jurkat, CEM, HuT78), NK cell lines (NK-92, NKL, YT, KHYG-1). D. Western blot demonstrating CTLA-4 expression in human NK cell lines. E. qrt-PCR demonstrating CTLA-4 expression in CD56+ selected ex vivo unstimulated NK cells derived from healthy human donors. Graphs are representative of 4 donors. F. Western blot of CTLA-4 expression in CD56+ selected ex vivo unstimulated NK cells derived from healthy human donors. Blots are representative of 4 donors.

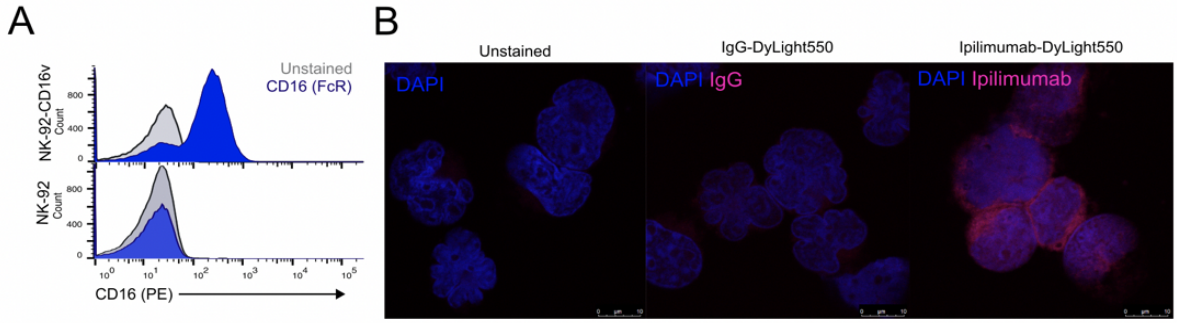

Figure 6: Ipilimumab binds to the NK cell surface independent of FcR. A. Flow cytometry demonstrating NK-92 does not express CD16. Positive control was the NK-92 line that had been transfected with a CD16 expressing plasmid, NK-92-CD16v. B. Immunofluorescent images of NK-92 cells stained with Dylight550-labelled ipilimumab demonstrating that ipilimumab binds to NK cell surface. Blue staining indicates DAPI. Shown are representative images of a single field of view taken via confocal microscopy (magnification, 63X, zoom, 3X).

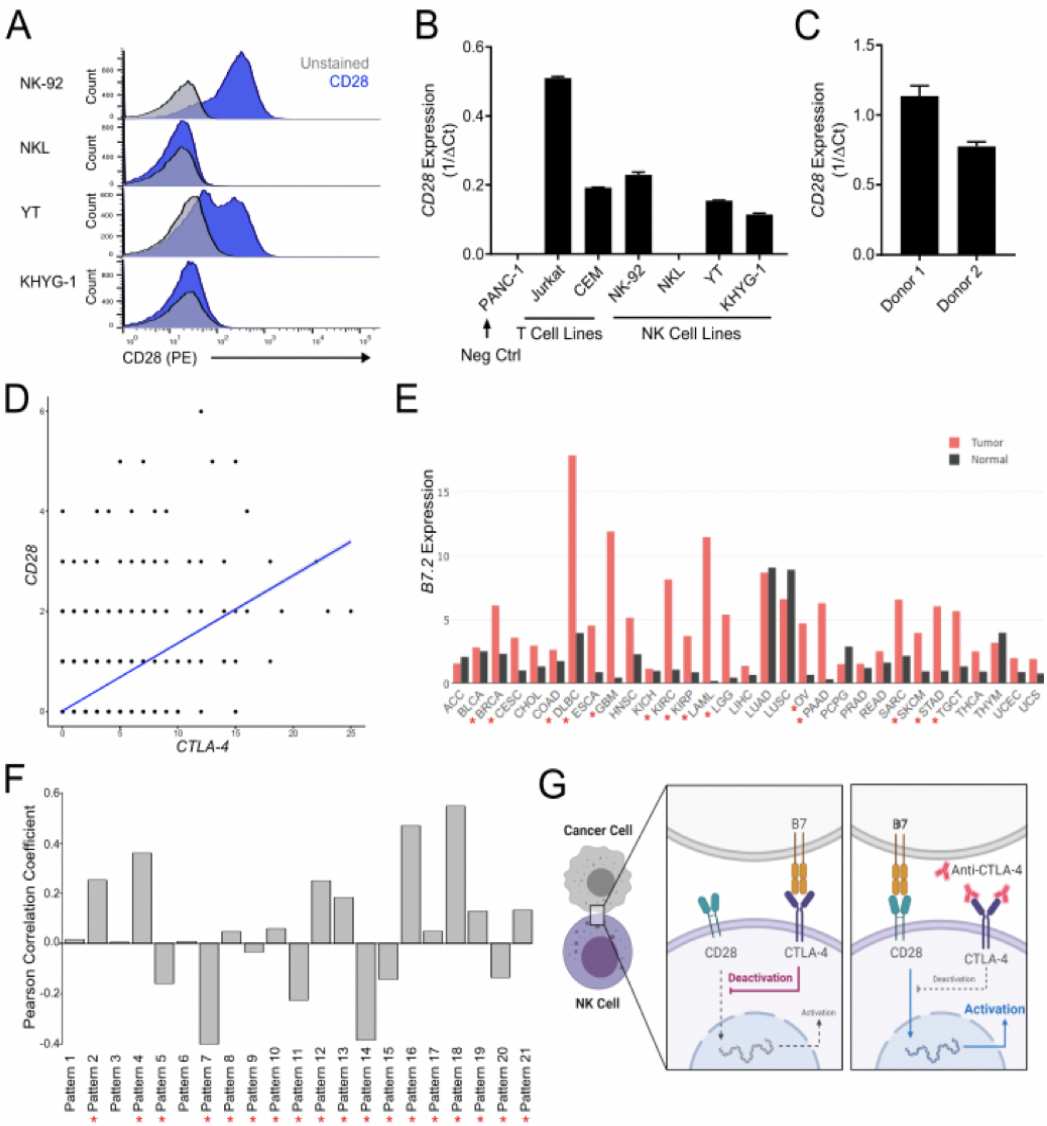

Figure 7: CD28 and CTLA-4 are coexpressed in circulating and tumoral NK cells. A. Flow cytometry for surface expression of CD28 in NK cell lines (NK-92, NKL, YT, KHYG-1). B. qRT-PCR analysis of CD28 expression in a CD28 null line (PANC-1), T cell lines (Jurkat, CEM), NK cell lines (NK-92, NKL, YT, KHYG-1). C. qRT-PCR demonstrating CD28 expression in CD56+ selected ex vivo unstimulated NK cells derived from PBMCs from healthy human donors. D. scRNAseq data demonstrating positive correlation (R^2 = 0.33, p = 0) between CD28 gene expression and CTLA-4 gene expression in human natural killer cells. E. B7.2 (CD86) mRNA expression levels in primary tumors versus paired normal (TCGA). Red asterisk (*) indicates cancer types with significantly overexpressed CD86 in tumor compared to normal tissue. F. Pan-cancer TCGA data demonstrating a negative correlation between pattern 7 weight and B7.2 expression. Significant correlation coefficients are indicated by a red asterisk (*). G. Schematic demonstrating proposed mechanism by which anti-CTLA-4 antibodies may enhance NK cell-mediated tumor clearance.

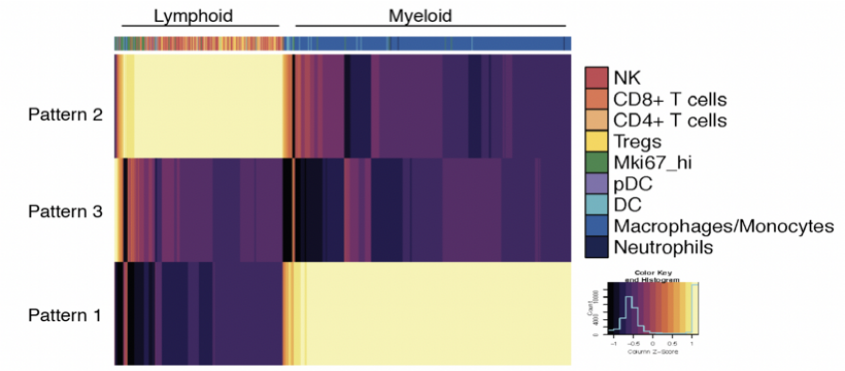

Supplemental Figure 1: CoGAPS identifies immune cell lineage at low dimensionality. When CoGAPS is performed at low dimensionality, here being 3 patterns, the identified signatures segregate cells by immune cell lineage. Pattern 3 is relatively flat across all cells, while 1 and 2 define myeloid and lymphoid lineage cells, respectively.

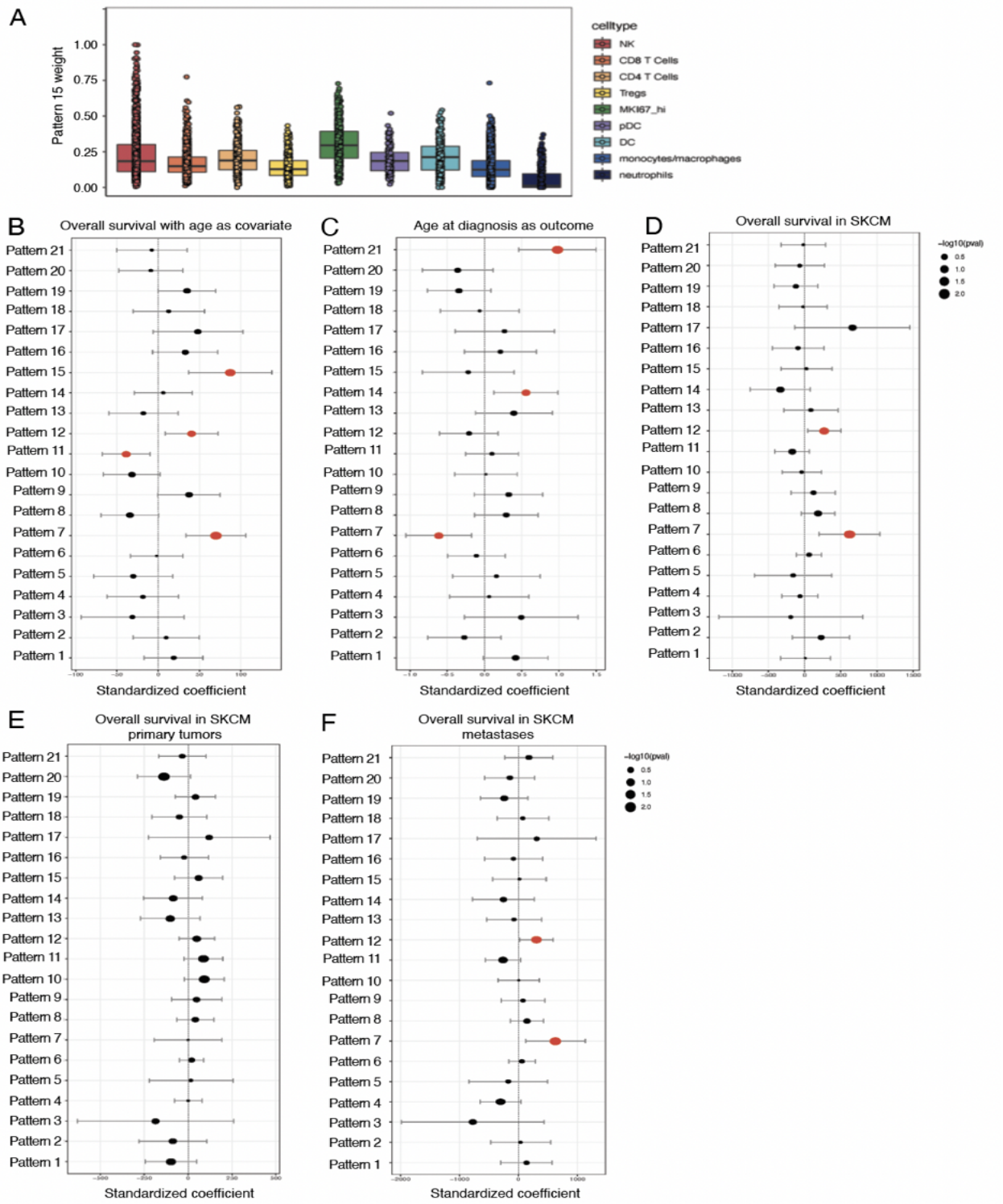

Supplemental Figure 2: Effect sizes of pattern associations with TCGA tumor survival. A. Boxplot of pattern 15 weights across each immune cell type from mouse sarcomas. Cells with the highest pattern 15 weights are observed in NK cells and Mki67hi proliferative lymphocytes. B. The output is shown from a multiple linear regression model that predicts overall tumor survival from our transcriptional patterns, while also adjusting for cancer type and patient age as covariates. Standardized coefficients (i.e. data was scaled and centered) representing the strength and direction of association for each pattern are shown on the xaxis, with error bars representing coefficient +- 1.96 * standard error, and point size scaled to the coefficient's p-value. Patterns 7 and 15 are most strongly positively associated with overall survival, with pattern 7 being most significantly positively associated ($p < 2.7 \times 10^{-4}$). C. The output is shown from a multiple linear regression model that predicts age of diagnosis from our transcriptional patterns, while also adjusting for cancer type as a covariate. ($p < 0.017$) D. The output is shown from a multiple linear regression model that predicts overall tumor survival in SKCM from our transcriptional patterns, while also adjusting for patient age as a covariate. Pattern 7 is the most significantly positively associated with overall survival in SKCM ($p < 0.005$). E. The output is shown from a multiple linear regression model that predicts overall tumor survival in SKCM primary tumors from our transcriptional patterns, while also adjusting for patient age as a covariate. Pattern 7 is not associated with overall survival in primary SKCM ($p > 0.05$). F. The output is shown from a multiple linear regression model that predicts overall tumor survival in SKCM metastases from our transcriptional patterns, while also adjusting for patient age as a covariate. Pattern 7 is the most significantly positively associated with overall survival in SKCM metastases ($p < 0.016$).

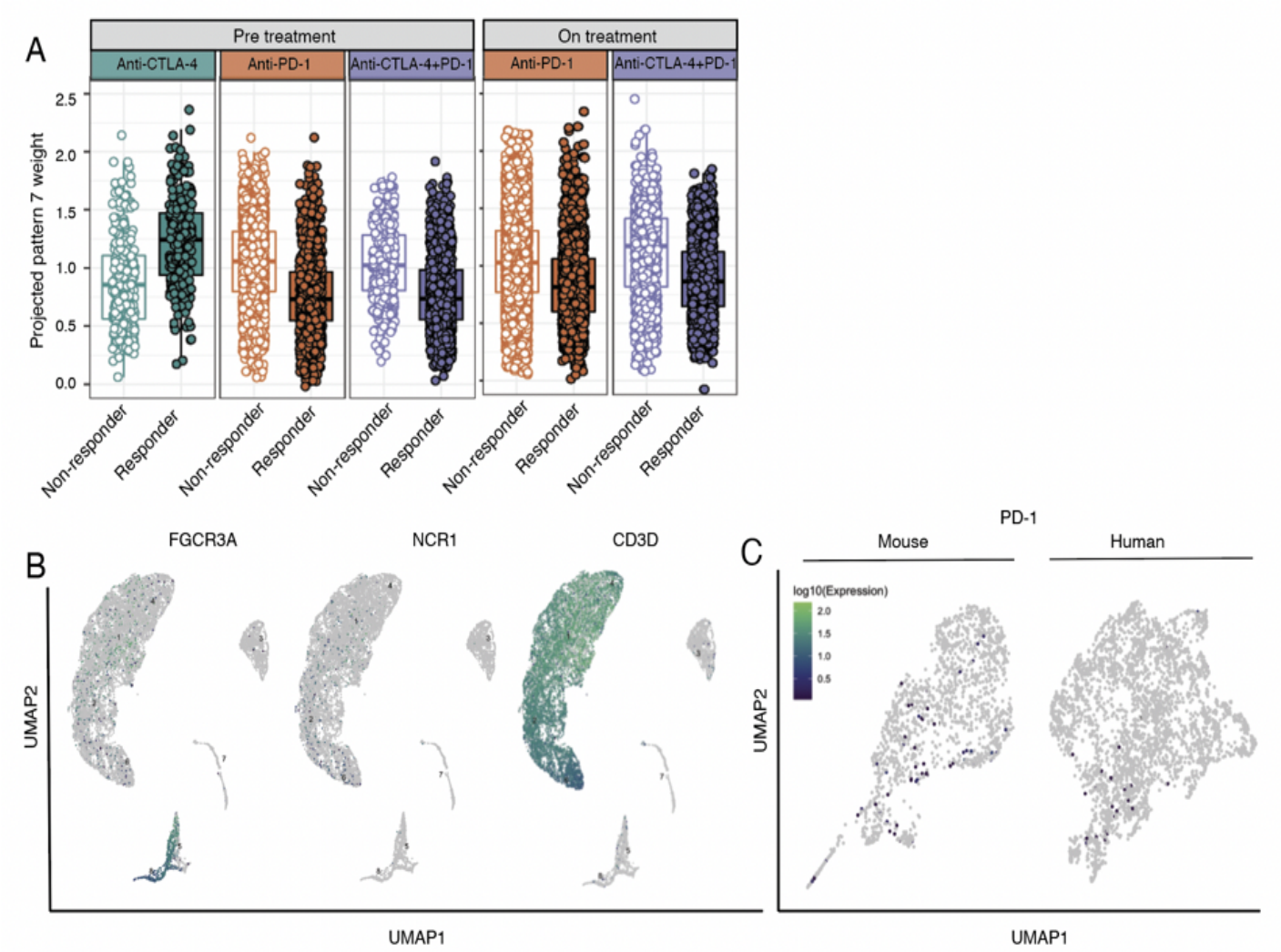

Supplemental Figure 3: NK cell activation signature is associated with anti-CTLA-4 response. A. Box plot of projected pattern 7 weights across intratumoral immune cells from metastatic melanoma patients prior to ICI treatment (Sade-Feldman et al., 2018). Cells are colored by therapy and separated by patient response. Increased pattern 7 is associated with immune cells from patients responsive to anti-CTLA-4. B. UMAP dimension reduction with cells colored by single-cell gene expression for representative NK and T cell marker genes. C. UMAP dimension reduction with cells colored by single-cell gene expression for PD-1 in mouse (left) and human (right) intratumoral NK cells. Activated NK cells are known to express PD-1, demonstrating that the observed pattern of PD-1 expression is consistent with the reduced ability of scRNA-seq to capture low to moderate expressed genes.

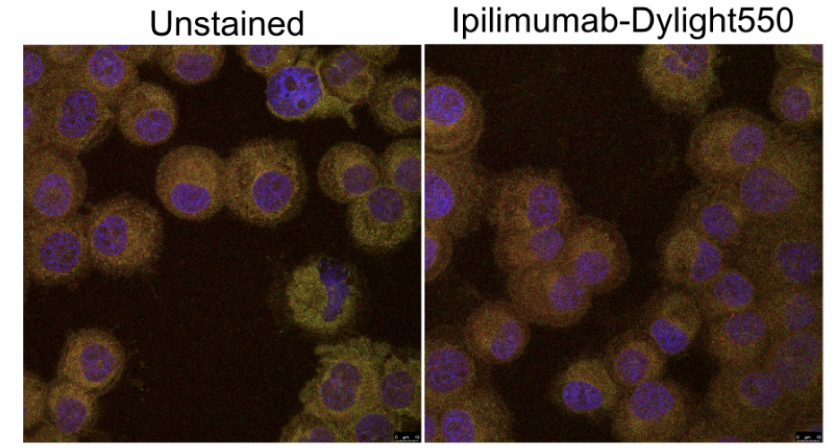

Supplemental Figure 4: Ipilimumab does not bind CTLA-4 null line PANC-1 Immunofluorescent images of PANC-1 cells stained with Dylight550-labelled ipilimumab. Blue staining indicates DAPI. Shown are representative images of a single field of view taken via confocal microscopy (magnification, 63X).

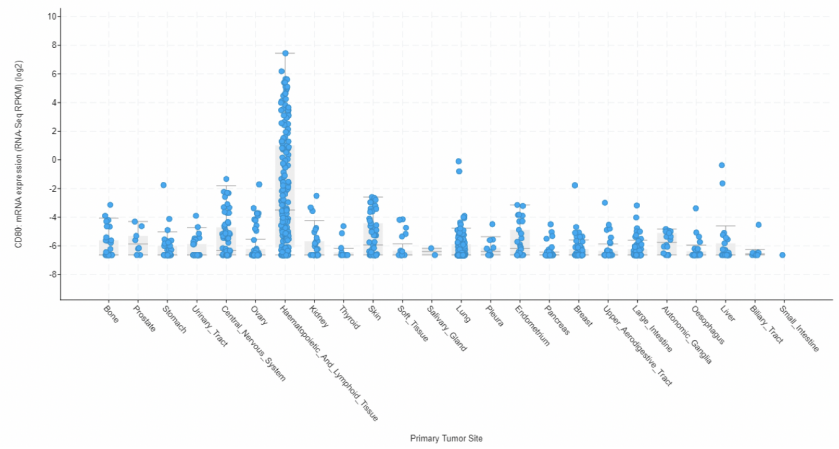

Supplemental Figure 5: CD80 expression in malignant cell lines. Data derived from CCLE RNAseq (Barretina et al. 2012; Gao et al. 2013).